The interplay between autophagy and the carbon/nitrogen ratio as key modulator of the auxin-dependent chloronema-caulonema developmental transition in *Physcomitrium patens*

Georgina Pettinari[1,2*], Franco Liberatore[1*], Veronica Mary[3], Martin Theumer[3], Ramiro Lascano[4,1], Laura Saavedra[1]

[1]Unidad Ejecutora de Doble Dependencia INTA-CONICET (UDEA), Córdoba, Argentina
[2]Current address: Linnean Center for Plant Biology, Swedish University of Agricultural Sciences, Uppsala BioCenter, Uppsala, Sweden
[3]Centro de Investigaciones en Bioquímica Clínica e Inmunología (CIBICI), Universidad Nacional de Córdoba-CONICET, Córdoba, Argentina
[4]Cátedra de Fisiología Vegetal, Facultad de Ciencias Exactas, Físicas y Naturales, Universidad Nacional de Córdoba, Córdoba, Argentina

* These authors contributed equally to this work

Authors for correspondence: Laura Saavedra, laura.saavedra@conicet.gov.ar, and Ramiro Lascano, ramiro.lascano@unc.edu.ar

ABSTRACT

Plant growth and development are tightly coordinated with metabolic status and environmental nutrient availability, yet how intracellular recycling pathways integrate these cues with hormonal signaling remains poorly understood outside angiosperms. Here, we used the model bryophyte *Physcomitrium patens* to address the role of autophagy in modulating auxin-induced caulonemata development in response to conditions altering the carbon/nitrogen (C/N) ratio. Loss of autophagic function enhanced caulonemata differentiation and colony expansion under ammonium-free and nitrogen-deficient conditions, phenocopying wild-type responses to nutrient starvation even under mild C/N imbalance. These developmental changes were associated with altered carbon homeostasis, increased endogenous indole-3-acetic acid (IAA) levels, reduced gene expression of the auxin exporter *PpPINA*, and up-regulation of auxin-responsive *RSL* transcription factors. In contrast, autophagy-deficient mutants show reduced sensitivity to exogenous sugars and exhibit hypersensitivity to prolonged auxin treatment, resulting in growth inhibition and cell death. Autophagic flux analyses revealed that caulonemata-inducing conditions, including auxin supply and nitrogen limitation, generally suppress autophagic activity, particularly during the dark period. Together, our results identify autophagy as a central integrator of metabolic and hormonal signals during early moss development, acting to restrain auxin-driven differentiation in favor of nutrient remobilization and growth homeostasis.

INTRODUCTION

As sessile organisms, plants must continuously sense and adjust their metabolism, physiology, morphology, growth and development to cope with changing environmental conditions. To achieve this, cells must remove damaged proteins, organelles and other debris that could cause malfunction, while recycling and replenishing nutrients to sustain their growth. Therefore, quality control systems, such as the ubiquitin/proteasome pathway and the autophagic route, are crucial for maintaining homeostasis and survival of plant cells. Whereas the former specializes in small, short-lived proteins, autophagy is the preferred degradative pathway for larger cytoplasmic material, such as organelles or protein aggregates (Dikic, 2017; Gross et al., 2025; Marshall & Vierstra, 2018; Petersen et al., 2024).

Autophagic induction in response to different stress conditions has been widely reported in plants (Avin-Wittenberg, 2019; Bassham et al., 2006; Filomeni et al., 2015; Jung et al., 2017; Kroemer et al., 2010; L.-Y. Lin et al., 2023; Y. Liu et al., 2009; Rose et al., 2006; Signorelli et al., 2019; Slavikova et al., 2008; Thirumalaikumar et al., 2021). It is also known that autophagy is activated during reprogramming events that take place after different internal and external stimuli, removing cellular components that are no longer needed to ensure proper execution of the new cell program (Kanne et al., 2022; Rodriguez et al., 2020). Autophagy is also induced by several processes associated with normal plant growth and development, such as the maintenance of energy availability during the night and the redistribution of nutrients during senescence (Avila-Ospina et al., 2014; Chen et al., 2019; Guiboileau et al., 2012; Izumi et al., 2013; Li et al., 2015; Y. Wang et al., 2013). In addition, autophagy is the main form of programmed cell death in plants, required for developmental processes such as xylem maturation, as well as the hypersensitive response to incompatible pathogens (Courtois-Moreau et al., 2009; Hofius et al., 2009; Liu et al., 2005; Üstün et al., 2017).

Most of our understanding of autophagy comes from studies in angiosperms; however, its integration with hormone signaling and nutritional stress remains poorly understood in other plant lineages. In this context, bryophytes are a particularly valuable group to study cellular processes involved in stress responses and homeostasis maintenance, such as autophagy, since they were the first group to successfully conquer the xeric, nutrient-poor terrestrial environment (Dong et al., 2025; Kürschner, 2004; McDaniel, 2021; Q.-H. Wang et al., 2022; Sakil 2025). Among them, the moss *Physcomitrium patens* has been widely established as a model organism for studying evolutionary plant cell biology and developmental processes (de Keijzer et al., 2021; Naramoto et al., 2022; Prigge & Bezanilla, 2010; Rensing et al., 2020). Understanding this connection in *P. patens* can provide insights into how stress and nutrient signaling networks evolved to coordinate growth and differentiation.

P. patens life cycle is predominantly haploid and begins with the germination of the spore to form a chloronemal initial cell. This chloronemal cell divides to produce chloronemal filaments, which can later differentiate into a caulonemal initial cell. Caulonemal cells also divide to form caulonemal filaments, from which secondary chloronemal or caulonemal branches are formed. Collectively, chloronemata and caulonemata are known as protonemata. Three-dimensional buds later emerge from caulonemal filaments and give rise to leafy

gametophores (Jaeger & Moody, 2021; Rensing et al., 2020). Chloronemal and caulonemal cells represent two different phases of *P. patens* filamentous growth. Both are tip-growing cells, yet they are morphologically and functionally distinct from one another (Menand et al., 2007b; Vidali & Bezanilla, 2012). Chloronemal cells can be considered as source tissues analogous to the leaves of vascular plants, since they actively perform photosynthesis and are rich in chloroplasts. In contrast, caulonemal cells are longer, faster-growing cells with fewer chloroplasts and colonizing functions. Thus, similar to the root hairs of vascular plants, caulonemata are responsible for substrate exploration and nutrient acquisition.

The transition from chloronema to caulonema is tightly regulated by auxins and depends not only on indole-3-acetic acid (IAA) accumulation but also on proper auxin sensing and signaling (Bascom et al., 2024; Nemec-Venza et al., 2022; Thelander et al., 2018, 2019). Caulonemata differentiation can also be induced by environmental factors such as light quality and nutrient availability. While nutrient-rich conditions and low light intensity favor chloronemata development, the transition to caulonemata is promoted when the plant faces nutritional deficiency (e.g., nitrogen or phosphorus starvation), or high energy availability conditions (such as high light intensity or glucose/sucrose supplementation) (Thelander et al., 2005). Interestingly, all of the above-mentioned conditions cause a carbon/nitrogen (C/N) imbalance, which is also known to modulate autophagic activity, raising the so far unexplored hypothesis of a connection among C/N ratio, autophagy, and caulonemata developmental transition.

Previous studies from our group demonstrated that *atg* mutants prioritize colony spread through filamentous growth, at the expense of reduced three-dimensional (3D) growth (buds and gametophores), thereby delaying the transition to the adult phase of the moss life cycle (Pettinari et al., 2022). We also showed that autophagy is induced in protonemata during the dark hours of a long-day photoperiod, as well as in response to nitrogen deficiency. In the present work, we assessed caulonemata development in autophagy-deficient mutants grown under different nutritional conditions in which the C/N ratio is affected, including sugar supplementation, ammonium-free media, and complete nitrogen starvation. Our results demonstrate that caulonemata differentiation is enhanced in *atg* mutants, thus phenocopying nitrogen starvation or sugar excess even under conditions that generate only mild C/N imbalances. Changes in caulonemata development correlate with an increase in IAA content and differential expression of auxin-related genes. Furthermore, we also detected alterations in endogenous sugar levels consistent with reduced sensitivity to exogenous sugar supply. Altogether, these findings indicate that autophagy could act as a central mechanism integrating cell metabolic status with hormonal signaling during the early developmental transitions of *P. patens*.

RESULTS

Autophagy-deficient mutants display enhanced colony expansion and sucrose accumulation under ammonium-free conditions

As a way to broadly evaluate caulonemata development, we first assessed the effect of autophagy deficiency on colony spread. To accomplish this, we grew equal amounts of protonematal inocula from WT and the previously characterized *atg5* and *atg7* mutants on BCD media containing only nitrate as a single nitrogen source. Although this medium does not impose a strong nutritional stress for WT plants, the absence of ammonium favors the transition from chloronemata to caulonemata, thus allowing for a better observation of this developmental process. After 19 days, the colony area of both *atg* mutant lines was significantly larger than in the WT (Figure 1-A). This spreading response phenocopies the known effect of complete nitrogen starvation on WT colonies, where caulonemata differentiation is further promoted to enhance substrate colonization and nutrient acquisition.

As mentioned, the transition from chloronemata to caulonemata is induced by auxin and sugar supplementation, among other factors. Previous data from our group revealed IAA accumulation in protonemata of *atg5* and *atg7* mutants grown in BCD (Pettinari et al., 2022), which is consistent with the enhanced colony expansion shown here. Considering that autophagy deficiency leads to alterations in cellular metabolism, which includes the C/N ratio, we set out to test whether endogenous sugar levels are effectively altered in these mutants. We measured glucose, sucrose, and fructose content in WT, *atg5* and *atg7* protonemata grown in BCD medium. We found that *atg* mutants accumulated significantly higher amounts of sucrose, while having lower glucose levels compared to the WT. No significant differences were detected in fructose content between genotypes (Figure 1-B). Altogether, these results suggest that the increased colony spread (and thereby, caulonemata development) of the autophagy-deficient mutants under ammonium-free conditions might be a consequence of an altered sugar profile, particularly the accumulation of sucrose, a transportable sugar which is known to promote caulonemata differentiation.

Colony expansion in atg mutants is less responsive to external sugar supply.

Given that *atg* mutants exhibited an altered sugar profile, we next explored the effect of increasing the C/N ratio through the addition of external sugars. Colony spread was evaluated in BCD media supplemented with different concentrations of glucose, sucrose or mannitol (Figure 2). As expected, in the WT, low to intermediate concentrations of glucose and sucrose stimulated colony expansion in comparison to the non-supplemented medium, with sucrose exerting a more pronounced effect. Similar responses were observed at 1% and 2,5% for each sugar. Interestingly, mannitol at these same concentrations also had a positive effect on colony spread, suggesting that it can either be assimilated by *P. patens* or that mild osmotic conditions favor colony spread. However, higher concentrations (5%) of glucose and mannitol reduced colony area compared to BCD, likely due to the osmotic stress effect. 5% sucrose still had a positive effect on growth, although values start to decrease after 14 days. Interestingly, this phenotypic response (colony expansion in the presence of sugars compared to the non-supplemented medium) was consistently lower in *atg5* and *atg7* mutants under all sugar treatments. This "hyposensitivity" to the application of sugars was particularly clear in the case of the sucrose supplemented media, specially the highest concentration tested (5%), where WT colonies were highly responsive while the autophagy-deficient lines were either non-responsive

or even showed a negative effect. The fact that *atg* mutants accumulate sucrose and show increased colony spread under non-supplemented media, but at the same time display a reduced spread response to the addition of exogenous sugars, particularly sucrose, indicates that the autophagic process could be a key coordinator of caulonemata development in response to changes in the carbon supply, which would in turn directly influence the internal C/N ratio.

Autophagy-deficient mutants show increased caulonemata development under nitrogen-deficient conditions

Since *PpATG5* and *PpATG7* encode proteins that participate in the same step of the autophagic process (i.e. ATG8 lipidation), we chose an additional *ATG* gene involved in a different step of autophagosome biogenesis to generate a third independent knockout line. Mutants lacking PpATG14, the differential subunit of the PI3K complex I, showed an intermediate senescent phenotype between the WT and *atg5* genotypes, consistently supported by chlorophyll content and cell death quantifications (Figures 3 and S1). Therefore, *atg14* mutants were included together with the *atg5* line in subsequent experiments.

To further investigate caulonemata development in *atg* mutants we performed a protoplast regeneration assay. Since it starts from a single cell, this type of assay allows for a more detailed observation of the chloronema-to-caulonema transition. In this case, we tested the effects of increasing the C/N ratio by lowering nitrogen availability in the media instead of adding sugars. Protoplasts were regenerated in nutrient-rich media (BCDAT, containing both ammonium and nitrate as nitrogen sources) until chloronemata filaments developed, and then transferred to two different caulonemata-inducing conditions: ammonium-free medium (BCD), and complete nitrogen deprivation (-N). Transference to fresh BCDAT media was used as a control. The percentage of caulonemata filaments was quantified 2 and 4 days after transference (Figure 4-A).

Nearly the same percentage of caulonemata filaments was observed in all genotypes under nutrient-rich conditions. Although a small but statistically significant difference between the WT and *atg* mutants was detected after 4 days, it appears to be negligible when compared with the effects observed under the other analyzed conditions. In ammonium-free medium (BCD), no changes were observed 2 days after transference compared to the control for any of the genotypes. After 4 days, however, all genotypes incremented the percentage of caulonemata filaments in this condition, with this increase being statistically higher in both *atg* mutants compared to the WT. Complete nitrogen deficiency (-N) triggered a rapid increase in the percentage of caulonemata filaments in all genotypes, with significantly higher values for *atg5* and intermediate values for *atg14* after just 2 days of transference to this medium. Prolonged exposure to this condition did not enhance caulonemata production in the WT any further, but at the same time, it erased the previously observed difference between genotypes. This effect might result from accelerated cell death caused by nitrogen deficiency in *atg* lines. Overall, these observations suggest that the differential caulonemata development occurred only in the first 2 days of exposure to complete nitrogen deprivation and that, even though *atg* mutants rapidly induce caulonemata development in this condition, they cannot sustain their growth over prolonged periods of time.

To further assess the progression of caulonemata differentiation we quantified the number of caulonemata cells per filament (Figure 4-B). This allowed us to identify in which genotypes or conditions the chloronema-to-caulonema differentiation is triggered earlier, indicated by the presence of a higher number of caulonemal cells per filament. Under nutrient-rich conditions (BCDAT), the WT genotype contained filaments with only one or two caulonemal cells, while the presence of filaments with up to three caulonemal cells was detected in both *atg* mutants. Intriguingly, this accelerated differentiation in the *atg* lines did not translate into a higher percentage of caulonemata filaments under nutrient-rich conditions, as mentioned earlier. Earlier differentiation was also observed in 3D growing structures of *atg* mutants, such as buds and gametophores (Figure S2-A), indicating that autophagy-deficient genotypes exhibit a generalized accelerated life cycle progression and consequently premature senescence. The ammonium-free condition (BCD) did not cause major changes in the WT compared to the nutrient-rich medium (BCDAT) during the evaluated period In contrast, filaments with up to three cells were observed in the mutants already after 2 days of growth in BCD, and filaments with four or more caulonemal cells developed in these genotypes after 4 days. Under complete nitrogen starvation (-N), the presence of filaments with four or more caulonemal cells was detected in all genotypes after just 2 days of exposure although a noticeably higher proportion was seen in the *atg* mutants. However, no further increases in this category of filaments was observed in the mutant lines after 4 days, while their number kept increasing in the WT.

Taken together, results obtained from the protoplast regeneration assays revealed that the absence of autophagy leads to accelerated caulonemata differentiation and a higher percentage of caulonemal filaments under nitrogen limitation (both ammonium or ammonium plus nitrate deficiencies). However, under complete nitrogen deprivation, this acceleration in the *atg* mutants appears to be short-lived, as caulonemal development became comparable among genotypes over time.

Exogenous auxin application leads to a potential toxic effect in the growth of atg mutants

As mentioned in the introduction, caulonemal development is tightly regulated by auxin signaling. To explore this modulation in the context of autophagic deficiency, the same protoplast regeneration analysis was used to evaluate caulonemata development in *atg* mutants after transference to auxin treatment (BCDAT + 1-naphthaleneacetic acid (NAA) 1 µM) (Figure 4-C). After 2 days, all lines slightly increased the percentage of caulonemata filaments compared to the treatment control (BCDAT), and no significant difference was observed between genotypes. However, while the WT maintained similar values of caulonemata development after 4 days, the percentage of caulonemata filaments in both *atg* mutants was reduced to control levels at this time point, possibly indicating the effect of auxin "wearing off". The number of caulonemata cells per filament observed after 2 days of auxin treatment was mostly similar to the control for each genotype, although the WT and *atg* mutants showed a slightly higher proportion of filaments with two and three caulonemal cells, respectively (Figure 4-D). However, this changed after 4 days of growth in NAA, when filaments with three caulonemal cells were found in the WT, while both mutant lines showed a reduction in this

category of filaments, interestingly reaching even lower levels than the control condition in *atg5*. Interestingly, while short auxin treatment had a similar developmental outcome in WT and mutant plants grown in microfluidic devices, autophagy-deficient lines showed growth arrest and a higher proportion of dead cells after longer exposures (Figure S2-B). Overall, these observations highlight time- and stage-dependent developmental effects of auxin and suggest a potential toxic effect in the growth of *atg* mutants over time.

Endogenous auxin homeostasis is altered in atg mutants

The effect of NAA supplementation in mutants with impaired autophagic activity suggests that endogenous auxin homeostasis is altered in these genotypes, thus explaining the potential toxic effect of external auxin supplementation. This is in correlation with previous work showing IAA accumulation in *atg5* and *atg7* mutants grown in BCD for 7 days (Pettinari et al., 2022). IAA quantification was repeated in this work using protonemata of *atg5* and *atg14* mutants grown in BCDAT for 4 days and then transferred to BCD or complete nitrogen deficiency (-N) (Figure 5), being directly comparable to the conditions used in the protoplast regeneration assay (Figure 4). Transference to a fresh BCDAT plate was used as a control. In the nutrient-rich medium (BCDAT), all genotypes showed similar IAA levels (Figure 5, BCDAT), with WT values comparable to previously reported levels for 5-7 days protonemata grown in BCDAT (Nemec-Venza et al., 2022; Ntefidou et al., 2023). A significant accumulation of IAA was detected in the *atg* mutant lines compared to the WT after transferring the tissue to both nitrogen-limited media (Figure 5, BCD and -N), with the highest values found in complete nitrogen deficiency. Interestingly, higher levels for *atg5* and intermediate values for *atg14* were observed in the two tested conditions, which is consistent with the previous intermediate phenotypes shown by *atg14*. These results point to alterations in endogenous auxin homeostasis linked to changes in the C/N ratio in the absence of autophagy.

Auxin-related gene expression is altered in autophagy-deficient mutants

To elucidate the cause behind the observed changes in IAA levels and caulonemata production in *atg* mutants, we evaluated the expression of auxin-related genes in nutrient-rich conditions (BCDAT) and after transference to ammonium-free media (BCD) (Figure 6). As an additional control, tissue was incubated with 5 µM NAA for 4.5 h to verify transcriptional responses to exogenous auxin (Bascom et al., 2023). Gene expression analysis was also performed after transferring the tissue to complete nitrogen deficiency. However, in this condition reference genes (*PpACT* and *PpADE-PRT*) showed markedly altered Ct values specifically in *atg* mutants, preventing reliable normalization and quantitative interpretation of the data. For this reason, complete nitrogen deficiency results are not shown. As discussed above, autophagy-deficient mutants undergo accelerated cell death when exposed to complete nitrogen deprivation, which is likely associated with a generalized alteration in transcriptional activity rather than gene-specific regulatory effects.

Genes encoding PpSHI1, a transcription factor (TF) that activates auxin biosynthesis genes, and PpYUCb, a YUCCA flavine monooxygenase, were chosen to analyze changes in auxin biosynthesis (Eklund et al., 2010a, 2010b; Landberg et al., 2021; Thelander et al., 2022).

Regarding transport, we evaluated the expression of *PpPINA*, which encodes the most abundant canonical PIN protein in *P. patens*, responsible for polar auxin transport towards the filament tip (Bennet et al., 2014; Fujita et al., 2008; Lüth et al., 2023; Viaene et al., 2014). We used *PpGH3-1* and *PpRSL* genes to assess auxin response and signaling. *PpGH3-1* is an auxin-inducible gene encoding an enzyme that catalyzes IAA conjugation to amino acids (Bierfreund et al., 2004). Although this gene is expressed both in protonemata and gametophores, the enzyme is only active in gametophores (Ludwig-Müller et al., 2009). Thus, increases in *PpGH3-1* expression in protonemata would indicate enhanced auxin response but not auxin inactivation. Members of the *RSL* (Root hair defective-Six Like) gene family were used as specific indicators of auxin-induced caulonemata development. These genes code for bHLH TFs that regulate the development of tip-growing cells involved in nutrient acquisition and rooting functions. Accordingly, these TFs control not only root hair development in flowering plants but also caulonemata and rhizoids development in *P. patens* (Jang et al., 2011; Jang & Dolan, 2011; Menand et al., 2007a; Pires et al., 2013). We analyzed the expression of two class I genes, *PpRSL1* and *PpRLS2*, and one class II gene, *PpRSL4*.

Under nutrient-rich conditions (BCDAT), expression of the biosynthesis-related genes, *PpSHI1* and *PpYUCb*, and of the auxin exporter *PpPINA* showed a significant increase in *atg* mutants compared to the WT. These observations suggest a possible regulatory loop in which the increase in auxin biosynthesis is counterbalanced with a higher export rate, thereby maintaining relatively constant IAA levels (similar to the ones found in the WT). This is consistent with the previously shown IAA measurements, where no differences were found among genotypes in BCDAT (Figure 5). On the other hand, *PpGH3-1* expression showed variable levels in *atg* mutants, with levels just slightly lower than the WT in *atg5* (although the difference is statistically significant) and markedly lower levels for *atg14*. This suggests that mutating different regulatory steps of autophagy results in different effects on auxin response, indicating a specificity for the control exerted by each component of autophagy in auxin signaling. Additionally, *RSL* genes exhibited different behaviours in the mutants, with higher expression for *RSL1*, lower expression for *RSL2* and values similar to the WT for *RSL4*. This opposite behavior shown by the class I *RSL* genes (*PpRSL1* and *PpRSL2*) suggests the presence of regulatory mechanisms to maintain stable levels in auxin-induced caulonemata production. Taken together with IAA quantification, the gene expression analysis would indicate that the accelerated life cycle of the *atg* mutants growing in nutrient-rich conditions (BCDAT) is not primarily driven by alterations in auxin content or signaling.

NAA treatment strongly induced *PpSHI1* and *PpYUCb* expression in the WT and *atg5*, while in *atg14* only *PpSHI1* was induced, not *PpYUCb*. Regarding transport, *PpPINA* expression increased in the WT but decreased in both *atg* mutants, resulting in significant differences between genotypes. As expected, after auxin treatment, *PpGH3-1* expression in the WT was higher than in the control medium. Although *PpGH3-1* levels in *atg5* mutants were also higher than in the control condition (WT, BCDAT), this increase was not as marked as in the WT. *PpGH3-1* expression in *atg14* mutants remained similar to the control. All analyzed *PpRSL* genes exhibited higher expression levels in the WT after auxin treatment compared to BCDAT. However, once again, each of these genes showed a different response in the

autophagy-deficient lines, with increased levels for *PpRSL1* and a decrease in *PpRSL2* and *PpRSL4*. Notably, *atg14* mutants presented intermediate levels for the three *RSL* genes. Differences detected in *PpGH3-1, PpRSL2* and *PpRSL4* expression levels between the WT and *atg* lines treated with exogenous NAA are consistent with the previously shown reduced caulonemata production in *atg5* and *atg14* plants (Figure 4-C and Figure 4-D).

After three days of growth in the ammonium-free condition (BCD), all genotypes showed increased levels of *PpSHI1* expression, whereas *PpYUCb* levels remained similar to the control (BCDAT). It is then possible that auxin biosynthesis levels are maintained by a regulatory loop acting downstream of *SHI1*, although it is also feasible that other *YUCs* rather than *YUCb* are involved in the response to ammonium deficiency. Interestingly, *PpPINA* expression in the WT did not change compared to the control condition, while its expression in the *atg* mutants was lower compared to the control condition. Once more, expression was significantly markedly lower than the WT in *atg5*, whilst *atg14* showed in-between values. Although PpPINA protein activity or accumulation was not analyzed, it is possible that the decrease in *PpPINA* gene expression is also reflected at the protein level, thus explaining the previously observed IAA accumulation in *atg* mutants transferred to BCD (Figure 5, BCD). Additionally, intermediate *PpPINA* expression levels in *atg14* mutants correlate with the intermediate IAA content found in this genotype compared to *atg5* and the WT.

Regarding auxin response genes in BCD, *PpGH3-1* levels in the WT were slightly lower than in BCDAT, although values for *atg* mutants did not differ from the control, and no statistical differences were found between genotypes. In the WT, expression of class I *RSL* genes (*PpRSL1* and *PpRSL2*) remained similar to the control condition, whereas *PpRSL4* decreased. Both *atg* mutants showed significantly higher expression for *PpRSL1* while *PpRSL4* levels were higher in *atg5* and intermediate in *atg14*. *PpRSL2* expression appeared to be lower in the mutants compared to the control condition, albeit no significant differences were detected between genotypes. These observations suggest that the enhanced caulonemata development previously observed in autophagy-deficient mutants would be mostly mediated by the induction of *PpRSL1* and, to a lesser extent, *PpRSL4,* as a consequence of IAA accumulation. Moreover, differences in IAA levels between *atg14* and *atg5* lines may also account for the observed difference in *PpRSL4* expression. However, this does not rule out the possibility that other class II *PpRSL* can contribute to the observed phenotype. Altogether, these results show that, in the absence of autophagy, auxin homeostasis and signaling appear to be differentially affected when plants are exposed to distinct caulonemata inducing conditions, which might explain the previously observed differences in caulonemata development between WT and *atg* lines.

Autophagic activity diminishes in caulonemata-inducing conditions

As shown by the results presented above, caulonemata development induced by nitrogen deficiency (either by the removal of ammonium or both ammonium and nitrate) is highly enhanced in mutants with impaired autophagic activity. In contrast, their response to exogenous auxin is lower compared to the WT, with their effect "wearing off" after some time. To understand the effect of these caulonemata inducing stimuli on actual autophagic activity, we performed a GFP-ATG8 cleavage assay using the PpATG8e::GFP-PpATG8e reporter line

(Sanchez Vera et al., 2017; Pettinari et al., 2022), to quantify autophagic flux following the transfer to different caulonemata-inducing conditions. For this assay, protonemata was grown for 3 days under nutrient-rich conditions (BCDAT) and then transferred to the different caulonemata inducing media: NAA, BCD or -N. Samples were collected across the second to fourth day after transference, at the end of both the light and dark periods of each day (with long-day photoperiod, 16:8h) (Figure 7). Exogenous auxin supply (BCDAT + NAA 1 μM) led to an immediate and sustained reduction of the autophagic flux compared to the control condition (BCDAT), an effect most clearly visible at the end of each dark period. This inhibition becomes more pronounced over time. The effect of ammonium deficiency (BCD) was more dynamic. Autophagic flux was reduced relative to BCDAT at the end of the light period on day two, but this trend reversed during the night, with flux remaining higher than the control until the end of day three. At that point, the effect reversed again, and autophagic flux stayed consistently lower than BCDAT at all subsequent time points. Finally, following transference to complete nitrogen deficiency (-N), autophagic flux gradually declined over time, with the strongest reduction by the end of each dark period. Altogether, these observations suggest that autophagy appears to have a higher activity across the day-night cycle in nutrient-rich conditions, while caulonemata-inducing conditions end up causing a decrease in autophagic activity, either immediately (strongly, NAA, or gradually, -N), or eventually (BCD).

DISCUSSION

In this study, we show that caulonemata development in *atg* mutants phenocopies the WT response associated with nitrogen deficiency even under mild C/N imbalances, such as the ammonium-free medium (BCD). Both, the protoplast regeneration assay and colony spread analysis indicate that nitrogen limitation induces earlier caulonema formation in *atg* mutants compared to the WT, highlighting an increased sensitivity of these genotypes to N availability. However, *atg* mutants were less responsive to the addition of exogenous sugars. Taken together, these results point to nitrogen availability (specifically, its deficiency) heavily influencing carbon metabolism in autophagic-deficient mutants. Previous studies showed impaired nitrogen metabolism in *P. patens* autophagy-deficient *atg3* genotypes (Chen et al., 2020), as well as down-regulation of enzymes involved in nitrogen assimilation in *Arabidopsis atg* mutants (James et al., 2025). Such defects may explain why the absence of ammonium is sufficient to trigger a pronounced developmental change in these mutants. Thus, we speculate that the addition of an external carbon source in the form of sugars does not influence the phenotype of the mutants as much as it does in the WT when there is a mild nitrogen deficiency (BCD, not enough to be stressful for the WT), because the main source of disruption in their metabolism comes specifically from issues in the assimilation or usage of nitrogen.

Upon nitrogen deficiency, WT *P. patens* plants deploy different strategies to obtain nutrients. On one hand, they might activate nutrient remobilization from source tissues (e.g., leaflets and chloronemal cells) to sink tissues (e.g., caulonemal cells and rhizoids) to sustain their growth. On the other hand, they could also alter their developmental program and promote caulonemata formation through the modulation of auxin signaling, thereby increasing substrate exploration. In either case, this could mean the activation of degradation routes of high nitrogen

containing organelles, like chlorophagy. Although autophagy-independent routes for chloroplast degradation have been reported in vascular plants (Wang & Blumwald, 2014; Zhuang & Jiang, 2019), there is no evidence yet that this is the case for *P. patens*. Consequently, if the plant facing this condition is an autophagy-deficient mutant, nutrient remobilization is most likely severely compromised. To compensate, *atg* plants cope with nutrient deficiency by increasing auxin-induced caulonemata development, as evidenced in the protoplast regeneration assay. Since the photosynthetically active chloronemata need a higher energy input and are more prone to redox damage under adverse conditions, increasing caulonemata development when facing a nitrogen deficiency probably serves as a strategy for *atg* mutants not only to search for nutrients but also to save up nitrogen and prevent oxidative damage, as they have fewer chloroplasts. Yet, this compensatory strategy most likely represents a short-term trade-off and would prove ultimately ineffective, as the energetic and metabolic imbalances caused by impaired autophagic activity inevitably lead to premature cell death. This energetic imbalance is also present in *P. patens* double mutants for the energy sensor SnRK1 (*Ppsnf1a-Ppsnafb*), which activates autophagy and inhibits the TOR complex. *Ppsnf1a-Ppsnafb* mutants display several developmental abnormalities, such as smaller gametophores, early senescence, reduced cytokinin sensitivity, enhanced auxin sensitivity, shorter chloronemal cells, and increased caulonemata development in BCD (Thelander et al., 2004). This phenotype closely resembles that of the *atg* mutants, although it is even more severe in the *SnRK1*-deficient lines (Pettinari et al., 2022; this work). While the authors associated caulonemata development with an intrinsical "high-energy growth" mode, in our work we highlight its association with increases in the C/N ratio, either by adding an external carbon supply or reducing nitrogen availability.

Our protoplast regeneration assay also showed that auxin supplementation failed to further induce caulonemata differentiation in *atg* mutants, but rather elicits a generalized negative effect in growth if treatment is prolonged over time. In this context, measuring auxin levels and analyzing auxin-related gene expression in different nutritional conditions provided valuable insight into how hormonal cues shape developmental responses to nutrient availability in autophagy-deficient mutants. Our RT-qPCR results showed that *PpPINA* expression is reduced in *atg* mutants upon transfer to the ammonium-free condition. If translated into a reduction in protein PpPINA expression/activity, this may generate a progressive intracellular auxin accumulation in the mutants, thus explaining the IAA accumulation detected in these genotypes. Moreover, in BCD media, *PpGH3-1* expression was similar between *atg* lines and WT, while *PpRSL1* and *PpRSL4* levels were higher in the mutants, indicating that auxin response is conserved and caulonemata development is enhanced in autophagy-deficient genotypes. This is in correlation with results obtained in the colony spread analysis and the protoplast regeneration assay in BCD.

A reduction in *PpPINA* expression compared to the WT was also observed in the mutant lines treated with exogenous auxin. However, BCD and NAA treatments had different effects on *atg* caulonemata development, with the former increasing its differentiation compared to the WT after 4 days, and a slight initial increase by the latter that rapidly wears off. This could be explained by the observed differences in the expression of auxin-response genes *PpGH3-1* and

PpRSLs. Additionally, it is well known that the effect of exogenous auxin supply on plant growth depends on concentration, duration and stage at which the treatment is applied (Asghar et al., 2023; Thelander et al., 2018). Thus, when *atg* mutants are incubated with NAA for longer periods of time, the increase in endogenous auxin levels due to lower export rates coupled to the incorporation of NAA from the media could surpass the growth-promoting intracellular auxin concentration threshold, leading to hypersensitivity and cell death. This hypothesis could account for the negative effect observed in cell survival after longer NAA exposures. In fact, it has been reported that overexpression of *PpSHI1* leads to an early senescence phenotype resembling that of *atg* mutants (Eklund et al., 2010). Considering that *atg* mutants growing in complete nitrogen deprivation showed the highest levels of IAA, auxin accumulation could also be contributing to the accelerated cell death of autophagy-deficient lines in this condition. Another scenario, where auxin production increases in dying cells as a consequence of tryptophan release during programmed cell death (PCD), has also been proposed (Sheldrake, 2021). Although autophagy is the main mechanism for PCD in plants, it has been reported that the 26S proteasome pathway is enhanced in *P. patens* mutants lacking *ATG3* to compensate for autophagy deficiency (Chen et al., 2020). Thus, ubiquitin-mediated protein degradation could be a possible source of tryptophan release and auxin production in the absence of autophagy. Whether early senescence in *atg* mutants is a cause or a consequence of IAA accumulation remains unexplored.

Noteworthily, the early senescence phenotype and developmental changes in *atg14* were not as severe as in the *atg5* line. This is an interesting observation, since phagophore decoration with PI3P (mediated by ATG14 as the autophagic subunit of PI3K complex I) and ATG8 lipidation (in which ATG5 is involved) are key processes that take place simultaneously during the progression of autophagy (Gross et al., 2025). However, this is not the first time that differences in the severity of the senescent phenotype have been observed among mutants of the autophagic machinery in plants, which do not necessarily correlate with the stage of the process in which each protein participates (Kang et al., 2018; Li et al., 2014; Suttangkakul et al., 2011). In general, less severe phenotypes are due to the presence of a multigenic family, although that is not the case for *PpATG14.* A plausible explanation for this could be found in the auxin-related results. IAA levels in *atg14* mutants showed intermediate values between the WT and the *atg5* genotype, and similar results were observed for auxin-related gene expression. In this regard, the previously mentioned study using mutants over-expressing *PpSHI1* found that higher expression levels led to a more pronounced senescent phenotype (Eklund et al., 2010), thus supporting the hypothesis of different levels of auxin content and sensitivity as the cause of the phenotypic differences found between *atg5* and *atg14* mutants.

Lastly, in this work, we demonstrated that exposure to media with a reduced nitrogen supply eventually results in a decrease in autophagic activity, this effect being either eventual or immediate depending on the type of deficiency (moderate or full), correlating with changes in cell type developmental programs across time. These results might initially seem inconsistent with our previous findings, where we demonstrated autophagic induction in protonemata cells under complete nitrogen deficiency (Pettinari et al., 2022). However, this does not necessarily represent a contradiction. Although nitrogen deprivation had effectively induced autophagy in

the two protonemal cell types, the number of autophagic particles in chloronemal apical cells was consistently higher than in caulonemal apical cells, both under nitrogen-sufficient (LN) and nitrogen-deficient (L–N) conditions. This observation suggests that higher autophagic activity is intrinsically associated with chloronemal tip cells regardless of nutrient status. Since nitrogen deficiency triggers developmental reprogramming towards caulonemata formation, the predominance of this cell type could explain the here-observed reduction in autophagic flux after transference to nitrogen-limited conditions. Nevertheless, this does not rule out the possibility that a certain level of autophagic activity can be activated to sustain the growth of caulonemal apical cells once they are formed. Recent studies have demonstrated that autophagy is required to promote root hair lifespan and pollen tube growth in vascular plants, which, like protonemata, depend on polar growth for their elongation (Feng et al., 2025; Yan et al., 2023). However, a key feature that sets apart moss protonemal cells from root hairs and pollen tubes is their ability to continue dividing throughout the moss life cycle, ultimately producing three-dimensional structures and allowing the cycle to continue (Rounds & Bezanilla, 2013). Autophagy serves as a key mechanism providing energy to sustain growth in the short term, which is highly important for short-lifespanned cells without chloroplasts like root hairs and pollen tubes. However, the autophagic process itself would not be enough to sustain protonemata growth under nutrient-limited conditions in the long term. Instead, the plant needs to change its developmental program and induce the transition from the photosynthetically active chloronemata to the colonizing caulonemata. Thus, these morpho-physiological differences among tip-growing cells indicate a need for cell-type-specific autophagic functions as part of the mechanisms activated to cope with changes in nutrient availability.

CONCLUSION

In this work we explored the interplay between autophagy, the C/N ratio, and the development of caulonemata in *Physcomitrium patens*. We demonstrated that autophagy deficient mutants display hypersensitivity to mild and complete nitrogen deficiency, manifested as an accelerated response in the transition from chloronemata to caulonemata development. At the same time, the mutants showed disrupted carbon metabolism, most interestingly evidenced by sucrose accumulation. This, in turn, probably resulted in a lessened response in caulonemata development when exposed to external sugars compared to the WT. At the same time, we demonstrated that enhanced caulonemata development in the mutants transferred to BCD positively correlates with IAA accumulation possibly due to reduced PIN expression, and increased expression of the auxin-responsive RSL genes that regulate the transition from chloronema to caulonema. We also found a generalized negative response to the addition of external auxin, suggesting that total intracellular auxin levels in the mutants surpass the growth-promoting threshold. Lastly, we demonstrated how these caulonemal inducing conditions generally diminish autophagic activity. In summary, we illustrated how the autophagic process is involved in the response to different conditions that disturb the C/N ratio and promote the developmental program of a nutrient-acquisition–focused cell type, the caulonemata, and how these responses and the metabolic state are massively disrupted in the absence of autophagy.

METHODS

Plant material and growth conditions

All experiments described in this study were performed with *Physcomitrium (Physcomitrella) patens ssp. patens* (Hedwig) ecotype 'Gransden 2004'. Plant cultures were grown axenically at 24°C under a long-day photoperiod (16-h light/8-h dark) with a photon flux of 60-80 $mmol.m^2.s^{-1}$. *P. patens* protonemal tissue from WT (wild type), *atg5*, *atg7* and *atg14* lines was subcultured routinely at 7-day intervals on cellophane disks (AA packaging) overlaying Petri dishes (90 mm in diameter) that contained BCDAT medium [0.92 g/L di-ammonium tartrate (C4H12N2O6), 0.25 g/L MgSO4.7H2O, 1.01 g/L KNO3, 0.0125 g/L FeSO4.7H2O, 0.25 g/L KH2PO4 (pH 6.5), 0.147 g/L CaCl2.2H2O, and 0.001% Trace Element Solution (0.055 g/L CuSO4.5H2O, 0.055 g/L ZnSO4.7H2O, 0.614 g/L H3BO3, 0.389 g/L MnCl2.4H2O, 0.055 g/L CoCl2.6H2O, 0.028 g/L KI, 0.025 g/L Na2MoO4.2H2O)] and 7 g/L agar.

Life cycle progression of the WT, *atg14* and *atg5* lines was observed using a microfluidic device with the help of Dr. Magdalena Bezanilla (Dartmouth College, Hanover, NH, USA). Homogenized protonemal tissue from WT, *Ppatg14-16*, and *Ppatg5* lines was loaded into the microfluidic chamber and incubated with Hoagland solution (Sigma-Aldrich, equivalent to liquid BCDAT medium) under continuous light for 21 days. The medium was then replaced with Hoagland solution supplemented with 1 µM NAA, and the tissue was incubated for an additional 15 days under these conditions. Tissue was imaged after 1, 5, 10, and 15 days of treatment (only images from days 5 and 15 are shown in Figure 4.4) using a Nikon Ti microscope equipped with a 20× objective (NA 0.8) and a Nikon DS-Vi1 color camera. Images were acquired every 20 min over a 24-h period, with the tissue continuously illuminated with white light.

Colony growth assay

For colony experiments in response to external sugars, moss colonies were initiated from 1 mm2 spot cultures (previously grown as protonema for 7 days in BCDAT medium) on cellophane overlaid BCD media (equivalent to BCDAT but with di-ammonium tartrate omitted), as well as BCD with added glucose, sucrose or mannitol, at three concentrations (1%, 2,5% or 5%). Three inoculi per genotype (WT, *atg5* and *atg7*) were placed on each Petri dish, and three dishes were used for each media. Colonies grew for 19 days, and they were imaged at 7 time points (days 0, 5, 7, 10, 12, 14, 19) using the GelDoc Go Gel Imaging System from BioRad. The images were processed using the scikit-image Python library, with which colony area was calculated. Representative images of moss colonies were imaged at day 19 of growth with an Olympus SZX16 stereomicroscope equipped with a color camera (Olympus DP71).

Quantification of soluble sugars via HPLC

Protonema of the WT, *atg5* and *atg7* genotypes were grown as previously described using BCD medium for 7 days. Tissue was harvested at the end of the light period of day 7, and was ground in liquid nitrogen in microtubes. Ethanol 80 % (4°C) was added in a w/v relation of 90 mg/750 µl, after which samples were incubated at 80°C for 30 min and then centrifuged at 14000 RPM for 10 min. The upper phase was collected, and one volume of pure acetonitrile was slowly added while on low shaking, after which the samples were left for 30 min at room temperature. Then samples were centrifuged at 14000 RPM for 15 min, the upper phase was collected and incubated at 90°C until evaporation. 500 µl of 75% acetonitrile was added, and samples were vortexed for 10 min. After that, samples were filtered using PDVF filters, and 10 µl were injected into an HPLC system. A Zorbax NH_2 column was used (4,6 mm x 250 mm x 5 µm) with an optimized flux of 1,5 µl/min, each sample being run for 30 min using a mobile phase of acetonitrile: water 70/30%. Times of retention were: fructose 4,6 min; glucose 5 min; sucrose 6,5 min. Results are shown as the area under the curve (AUC).

Generation and identification of *Ppatg14* knock-out mutants

The atg14-ko vector for generating mutants by homologous recombination was constructed by cloning approximately 1000 bp from the 5' and 3' ends of the *PpATG14* gene into a pUBW302 plasmid with G418 resistance. The resulting vector was linearized using the restriction enzymes XhoI and XbaI and introduced into WT by polyethylene glycol–mediated protoplast transformation according to Saavedra et al., 2015. Briefly, 6-day-old protonemal tissue from WT was incubated under gentle agitation (approximately 20 rpm) with Driselase (Sigma-Aldrich) for 45 min at room temperature. Driselase was at a concentration of 1 % (w/v) dissolved in 8.5% (w/v) mannitol. The resulting protoplasts were filtered using a 100-µm mesh filter and washed three times with 8.5% (w/v) mannitol by centrifugation at 600 rpm. For each transformation, 0.3 ml of protoplasts at a density of 1.6×10^6 protoplasts/ml, 10–15 µg of linear DNA from the plasmid of interest, and 0.3 ml of PEG solution (8.5% [w/v] mannitol, 1% [v/v] 1 M Ca(NO3)2, 0.1% [v/v] 1 M Tris-Cl pH 8.0, and 4 g PEG 4000) were used. Transformed protoplasts were then plated on Petri dishes containing PMRB medium (0.5 g/L di-ammonium tartrate, 0.25 g/L MgSO4.7H2O, 0.0125 g/L FeSO4.7H2O, 0.8 g/L CaNO3.4H2O, 0.25 g/L KH2PO4 pH 6.5, 0.001% Trace Element Solution, 60 g/L mannitol, and 7 g/L agar). For each plate, 500 µl of transformed protoplasts were mixed with 500 µl of PMRT medium (PMRB medium with instead 80 g/L mannitol and 1.5 g/L agar). After 7 days, the resulting *P. patens* colonies were subjected to two rounds of selection on solid BCDAT medium supplemented with G418 at 40 µg/ml to eliminate potential resistance caused by the presence of plasmid DNA not integrated into the *P. patens* genome. Mutants were identified through 2 consecutive rounds of genotyping. In the first round, primers binding the deleted region were used, and plants failing to amplify this region were selected for further analysis. For the second round, pairs of primers with one oligo binding outside the homology regions present in the vector were used to ensure the correct insertion of the plasmid into the genome. *PpATG14* expression levels in

atg14-16 and *atg14-34* lines were evaluated using RT-qPCR (see Quantification of auxin-related gene expression for details on RNA extraction, cDNA synthesis and qPCR protocol).

Determination of chlorophyll content and quantification of cell death

Total chlorophyll content was quantified using 28-day-old colonies grown without cellophane on BCDAT and BCD media. In this case, pigments were extracted with 80% (v/v) acetone. Chlorophylls were quantified by spectrophotometry at 664 nm and 648 nm. Determinations were performed in triplicate. Calculations were performed using the following equation: Chla ug.ml-1= [(12.25 · Abs664) – (2.79 ·Abs648)] ; Chlb ug.ml-1= [(21.5 ·Abs648) – (5.10 · Abs664)]. For cell death quantification, 28d colonies grown on solid BCD medium without cellophane were incubated in 1.5-ml Eppendorf tubes with 0.05% Evans Blue for 2 h. Subsequently, four washes with distilled water were performed to remove excess stain. The dye bound to dead cells was solubilized in 50% methanol containing 1% SDS for 45 min at 50°C. Each biological replicate consisted of three colonies incubated with 2 ml of the methanol/SDS mixture, and three replicates were analyzed per condition. For each replicate, a 300-µl aliquot was transferred to a well of a 96-well multiwell plate to measure absorbance at 600 nm. The dry weight of the colonies was determined after completion of the procedure by drying the plants for 18 h at 65°C. Results are expressed as OD_{600} per gram of dry weight.

Protoplasts regeneration and caulonemata development analysis

Protoplasts from WT, *atg14-16,* and *atg5* lines were obtained following the protocol for plant transformation mentioned above. After the mannitol washes, protoplasts were resuspended in PMRT medium at a density of 2 × 10^4 protoplasts per ml, and 1 ml of this solution was plated into Petri dishes containing PMRB medium and cellophane. After 2 days in PMRB, regenerating protoplasts were transferred to BCDAT for 48 h. Next, cellophanes were moved to the following caulonemata-inducing treatments: 1) new BCDAT plate (control, nutrient-rich); 2) BCD (+NO_3, -NH_4. BCDAT without di-ammonium tartrate), auxin treatment (BCDAT + NAA 1 mM); 4) complete nitrogen deficiency (-N: -NO_3, -NH_4. BCD in which KNO3 was replaced by 1.41 g/L NaK tartrate). Tissue was observed after 2 and 4 days of treatment using an Olympus BX-61 microscope equipped with an Olympus DP71 color camera. Between 50 and 60 filaments were quantified per condition, and the experiment was repeated three times. For quantification, only the main filaments with a minimum length of three cells were considered. Two parameters were recorded: (1) the total number of filaments containing at least one caulonemal cell, and (2) the number of caulonemal cells in each filament analyzed. For each timepoint, values for every treatment and genotype are shown as relative to the percentage of the WT in BCDAT (control condition). The number of filaments containing 1, 2, 3, and 4 or more caulonemal cells is expressed as a proportion of the total number of caulonemal filaments observed in each combination of treatment and time point.

IAA quantification

Hormone levels in 7d protonemal tissue from WT, *atg5*, and *atg14* lines were quantified by liquid chromatography–tandem mass spectrometry (LC–MS/MS). Tissue was grown during 4 days on BCDAT with cellophane and then transferred to BCD, -N or a new BCDAT plate (control) for 3 additional days. Three biological replicates were analyzed for each genotype. For hormone extraction, 100 mg of tissue previously ground in liquid nitrogen was homogenized with 500 µl of a 1-propanol/H2O/concentrated HCl solution (2:1:0.002, v/v/v) by shaking at 4°C for 30 min. Subsequently, 1 ml of dichloromethane (CH2Cl2) was added to each sample, followed by further homogenization by shaking at 4°C for 30 min and centrifugation for 5 min at 13,000 × g. The lower organic phase (approximately 1 ml) was collected into glass vials and evaporated under a nitrogen stream. Samples were then re-dissolved in 0.25 ml of a solution containing 50% methanol (HPLC grade) with 0.1% formic acid and 50% H2O with 0.1% formic acid using a vortex mixer.

Chromatographic analyses were performed using an LC–MS system (Waters Xevo TQ-S Micro, Waters, Milford, MA, USA) equipped with a quaternary pump (Acquity UPLC H-Class, Waters), an autosampler (Acquity UPLC H-Class, Waters), and a reverse-phase column (Waters BEH C18, 1.7 µm, 2.1 × 50 mm). The mobile phase consisted of water with 0.1% formic acid (A) and methanol with 0.1% formic acid (B), with a flow rate of 0.25 ml/min. The initial gradient was held at 40% B for 30 s, then increased linearly to 100% B and maintained for 3 min. IAA identification and quantification were performed using a Xevo TQ-S Micro mass spectrometer (Waters, Milford, MA, USA) coupled to the UPLC system. Electrospray ionization (ESI) was used as the ion source, and mass spectra were acquired in positive ion mode. Data acquisition and processing were carried out using MassLynx software (version 4.1). The mass-to-charge (m/z) transitions monitored were 176.0 → 103.0 and 176.0 → 130.0. Quantification was performed using calibration curves with linear regression, and results are expressed as ng of phytohormone per g of fresh weight. For each condition, values for all genotypes are shown as relative to the WT in the same condition.

Quantification of auxin-related gene expression

Homogenized protonemata from WT, *atg5* and *atg14-16* lines were grown in BCDAT for 4 days and then transferred to the following caulonemata-inducing conditions for 3 additional days: 1) new fresh BCDAT plate (control); 2) BCDAT + NAA 5 mM (tissue was placed in a second BCDAT plate for 3 days and 4.5 h prior to collection it was transferred to a third BCDAT plate supplemented with NAA); BCD (+NO_3, -NH_4); -N (-NO_3, -NH_4). Treatments were carried out in triplicates and all samples were collected 7 days after homogenization. Total RNA was extracted using Quick-Zol (Kalium Technologies) according to the manufacturer's instructions. 2 mg per sample of total RNA was treated with 2 units of DNAse I (Thermo Fisher Scientific) and used as template for cDNA synthesis. RevertAid Transcriptase (Thermo Fisher Scientific) and oligo-dTs were used according to the manufacturer's protocol. The quantitative PCR reaction was carried out in LineGene 9600 Plus Fluorescence Quantitative Detection System using EvaGreen® (Genbiotech) and Dream Taq

(Thermo Fisher Scientific). Actin and Ade-PRT were used as reference genes to normalize the samples. For each gene and condition, values are shown as relative to the WT in BCDAT (control condition).

Autophagic flux assay via immunoblotting

Protonema of the reporter line PpATG8epro:GFP-PpATG8e was grown on cellophane disks overlaid on solid BCDAT media, inside sterile 12-well multiwell plates. The tissue was grown for 4 days on BCDAT media and then transferred to solid media: BCDAT, BCDAT + NAA, BCD, or -N (where the ammonium tartrate and potassium nitrate of BCDAT media were omitted and substituted by potassium tartrate). Samples were harvested at the indicated time points, both at the end of the light or the dark period of the different days after transference to treatment. Samples were ground in liquid nitrogen in 1,5 ml microtubes using pestle pellets, and 50 µl of protein extraction buffer was added (100 mM Tris-HCl, 1 mM EDTA, 2% SDS, 100 mM NaCl, 1 mM PMSF, and 25X protease inhibitor Complete Roche). Samples were centrifuged at 13000 RPM for 10 min, the protein-containing upper phase was collected, and protein concentration was measured using the Lowry method using a SYNERGY H1 microplate reader, from Biotek. Samples (20 ug of protein) were separated in an electrophoretic run, using 12% acrilamide SDS-PAGE gels, after which proteins were transferred to a PVDF membrane. Equal sampling was ensured by 0,5 % Ponceau S staining, and membranes were blocked for 1 hour in TBS-T buffer (50 mM Tris-HCl, 150 mM NaCl, 0,1% Tween20, pH 7.5) with 5% skimmed milk, after which membranes were washed with TBS-T once for 15 min and twice for 10 min. They were incubated overnight at 4°C with anti-GFP antibody 1:5000 in TBS-T (Agrisera Rabbit αGFP AS20). Membranes were washed again and then incubated at RT for 1 hour with secondary antibody 1:10000 (αRabbit igG Alkaline Phosphatase Conjugate SIGMA A-3687). They were washed again and incubated with AP-revealing solution (Tris-Cl 100 mM, MgCl2 5 mM, NBT 0,033%, and BCIP 0,015%). The membranes were imaged using the GelDoc Go Gel Imaging System from BioRad, and bands were quantified using image analysis libraries from Python (scikit-image). Autophagic flux was determined as the ratio between free GFP and the sum of free GFP and GFP-ATG8e.

Authors contribution

G.P: Conceptualization, experimental design, performed experiments, formal analysis, and writing - original draft, Writing - review & editing**.** FL: Conceptualization, experimental design, performed experiments, formal analysis, and writing - original draft, Writing - review & editing**.** VM: Performed hormone quantification**.** MT: Performed hormone quantification**.** RL: Conceptualization, experimental design, funding acquisition, supervision, project administration, validation, writing - review & editing**.** LS: Conceptualization, experimental design, performed experiments, formal analysis, funding acquisition, supervision, project administration, validation, writing - review & editing

Funding

This work was supported by grants from Agencia Nacional de Promoción Científica y Tecnológica, Argentina FONCYT-PICT2020-2482 to L.S, PIBAA-28720210100691CO01 (CONICET) to L.S, FONCYT-PICT-2019-00533 to R.L, Proyectos Consolidar, Secretaría de Ciencia y Técnica de la Universidad Nacional de Córdoba (UNC) to R.L and Proyecto INTA 2023-PD-L03-I084 (to L.S and R.L).

Acknowledgments

We acknowledge CONICET for the Ph.D. scholarships to G.P and to F.L, and the Fulbright Commission and CFI Argentina for the FLB-CFI-2023-2024 research grant to G.P. We acknowledge Dr. Virginia Lobatto and Dr. Esteban Schenfield for technical support.

Conflict of interest

The authors declare that the research was conducted in the absence of any commercial or financial relationships that could be construed as a potential conflict of interest.

REFERENCES

Asghar, S., Ghori, N., Hyat, F., Li, Y., & Chen, C. (2023). Use of auxin and cytokinin for somatic embryogenesis in plant: A story from competence towards completion. *Plant Growth Regulation*, *99*(3), 413–428. https://doi.org/10.1007/s10725-022-00923-9

Avila-Ospina, L., Moison, M., Yoshimoto, K., & Masclaux-Daubresse, C. (2014). Autophagy, plant senescence, and nutrient recycling. *Journal of Experimental Botany*, *65*(14), 3799–3811. https://doi.org/10.1093/jxb/eru039

Avin-Wittenberg, T. (2019). Autophagy and its role in plant abiotic stress management. *Plant, Cell & Environment*, *42*(3), 1045–1053. https://doi.org/10.1111/pce.13404

Bascom, C., Jr, Prigge, M. J., Szutu, W., Bantle, A., Irmak, S., Tu, D., & Estelle, M. (2023). Clade-D auxin response factors regulate auxin signaling and development in the moss Physcomitrium patens. *PLOS Biology*, *21*(6), e3002163. https://doi.org/10.1371/journal.pbio.3002163

Bascom, C., Jr, Tu, D., Repakula, S., Prigge, M. J., & Estelle, M. (2025). The role of auxin-mediated gene activation in the bryophyte, Physcomitrium patens. *Journal of Experimental Botany*, *76*(14), 4043–4054. https://doi.org/10.1093/jxb/eraf183

Bassham, D. C., Laporte, M., Marty, F., Moriyasu, Y., Ohsumi, Y., Olsen, L. J., & Yoshimoto, K. (2006). Autophagy in Development and Stress Responses of Plants. *Autophagy*, *2*(1), 2–11. https://doi.org/10.4161/auto.2092

Bennett, T. A., Liu, M. M., Aoyama, T., Bierfreund, N. M., Braun, M., Coudert, Y., Dennis, R. J., O'Connor, D., Wang, X. Y., White, C. D., Decker, E. L., Reski, R., & Harrison, C. J. (2014). Plasma Membrane-Targeted PIN Proteins Drive Shoot Development in a Moss. *Current Biology*, *24*(23), 2776–2785. https://doi.org/10.1016/j.cub.2014.09.054

Bierfreund, N. M., Tintelnot, S., Reski, R., & Decker, E. L. (2004). Loss of *GH3* function does not affect phytochrome-mediated development in a moss, *Physcomitrella patens*. *Journal of Plant Physiology*, *161*(7), 823–835. https://doi.org/10.1016/j.jplph.2003.12.010

Chen, Q., Shinozaki, D., Luo, J., Pottier, M., Havé, M., Marmagne, A., Reisdorf-Cren, M., Chardon, F., Thomine, S., Yoshimoto, K., & Masclaux-Daubresse, C. (2019). Autophagy and Nutrients Management in Plants. *Cells*, *8*(11), 1426. https://doi.org/10.3390/cells8111426

Chen, Z., Wang, W., Pu, X., Dong, X., Gao, B., Li, P., Jia, Y., Liu, A., & Liu, L. (2020). Comprehensive analysis of the Ppatg3 mutant reveals that autophagy plays important roles in gametophore senescence in Physcomitrella patens. *BMC Plant Biology*, *20*(1), 440. https://doi.org/10.1186/s12870-020-02651-6

Courtois-Moreau, C. L., Pesquet, E., Sjödin, A., Muñiz, L., Bollhöner, B., Kaneda, M., Samuels, L., Jansson, S., & Tuominen, H. (2009). A unique program for cell death in xylem fibers of Populus stem. *The Plant Journal*, *58*(2), 260–274. https://doi.org/10.1111/j.1365-313X.2008.03777.x

de Keijzer, J., Freire Rios, A., & Willemsen, V. (2021). Physcomitrium patens: A Single Model to Study Oriented Cell Divisions in 1D to 3D Patterning. *International Journal of Molecular Sciences*, *22*(5), 2626. https://doi.org/10.3390/ijms22052626

Dikic, I. (2017). Proteasomal and Autophagic Degradation Systems. *Annual Review of Biochemistry*, *86*(Volume 86, 2017), 193–224. https://doi.org/10.1146/annurev-biochem-061516-044908

Dong, S., Wang, S., Li, L., Yu, J., Zhang, Y., Xue, J.-Y., Chen, H., Ma, J., Zeng, Y., Cai, Y., Huang, W., Zhou, X., Wu, J., Li, J., Yao, Y., Hu, R., Zhao, T., Villarreal A, J. C., Dirick, L., … Liu, Y. (2025). Bryophytes hold a larger gene family space than vascular plants. *Nature Genetics*, *57*(10), 2562–2569. https://doi.org/10.1038/s41588-025-02325-9

Eklund, D. M., StÅldal, V., Valsecchi, I., Cierlik, I., Eriksson, C., Hiratsu, K., Ohme-Takagi, M., Sundström, J. F., Thelander, M., Ezcurra, I., & Sundberg, E. (2010a). The Arabidopsis thaliana STYLISH1 Protein Acts as a Transcriptional Activator Regulating Auxin Biosynthesis. *The Plant Cell*, *22*(2), 349–363. https://doi.org/10.1105/tpc.108.064816

Eklund, D. M., Thelander, M., Landberg, K., Ståldal, V., Nilsson, A., Johansson, M., Valsecchi, I., Pederson, E. R. A., Kowalczyk, M., Ljung, K., Ronne, H., & Sundberg, E. (2010b). Homologues of the Arabidopsis thaliana SHI/STY/LRP1 genes control auxin biosynthesis and affect growth and development in the moss Physcomitrella patens. *Development*, *137*(8), 1275–1284. https://doi.org/10.1242/dev.039594

Feng, Q., Zhu, S., Wang, X., Liu, Y., Zhao, J., Dagdas, Y., & Nowack, M. K. (2025). Root hair lifespan is antagonistically controlled by autophagy and programmed cell death (p. 2025.03.18.643910). bioRxiv. https://doi.org/10.1101/2025.03.18.643910

Filomeni, G., De Zio, D., & Cecconi, F. (2015). Oxidative stress and autophagy: The clash between damage and metabolic needs. *Cell Death & Differentiation*, *22*(3), 377–388. https://doi.org/10.1038/cdd.2014.150

Fujita, T., Sakaguchi, H., Hiwatashi, Y., Wagstaff, S. J., Ito, M., Deguchi, H., Sato, T., & Hasebe, M. (2008). Convergent evolution of shoots in land plants: Lack of auxin polar transport in moss shoots. *Evolution & Development*, *10*(2), 176–186. https://doi.org/10.1111/j.1525-142X.2008.00225.x

Gross, A. S., Raffeiner, M., Zeng, Y., Üstün, S., & Dagdas, Y. (2025). Autophagy in Plant Health and Disease. *Annual Review of Plant Biology*, *76*(Volume 76, 2025), 197–227. https://doi.org/10.1146/annurev-arplant-060324-094912

Guiboileau, A., Yoshimoto, K., Soulay, F., Bataillé, M.-P., Avice, J.-C., & Masclaux-Daubresse, C. (2012). Autophagy machinery controls nitrogen remobilization at the whole-plant level under both limiting and ample nitrate conditions in Arabidopsis. *New Phytologist*, *194*(3), 732–740. https://doi.org/10.1111/j.1469-8137.2012.04084.x

Hofius, D., Schultz-Larsen, T., Joensen, J., Tsitsigiannis, D. I., Petersen, N. H. T., Mattsson, O., Jørgensen, L. B., Jones, J. D. G., Mundy, J., & Petersen, M. (2009). Autophagic Components Contribute to Hypersensitive Cell Death in Arabidopsis. *Cell*, *137*(4), 773–783. https://doi.org/10.1016/j.cell.2009.02.036

Izumi, M., Hidema, J., Makino, A., & Ishida, H. (2013). Autophagy Contributes to Nighttime Energy Availability for Growth in Arabidopsis. *Plant Physiology*, *161*(4), 1682–1693. https://doi.org/10.1104/pp.113.215632

Jaeger, R., & Moody, L. A. (2021). A fundamental developmental transition in Physcomitrium patens is regulated by evolutionarily conserved mechanisms. *Evolution & Development*, *23*(3), 123–136. https://doi.org/10.1111/ede.12376

James, M., Trouverie, J., Bernay, B., Marmagne, A., Chardon, F., Gemin, M.-P., Etienne, P., & Masclaux-Daubresse, C. (2025). V-ATPases and amino acid catabolism are strongly disturbed in the roots of autophagy mutants in Arabidopsis, impacting water use efficiency and tricarboxylic acid metabolism. *The Plant Journal*, *123*(2), e70359. https://doi.org/10.1111/tpj.70359

Jang, G., & Dolan, L. (2011). Auxin promotes the transition from chloronema to caulonema in moss protonema by positively regulating PpRSL1 and PpRSL2 in Physcomitrella patens. *New Phytologist*, *192*(2), 319–327. https://doi.org/10.1111/j.1469-8137.2011.03805.x

Jang, G., Yi, K., Pires, N. D., Menand, B., & Dolan, L. (2011). RSL genes are sufficient for rhizoid system development in early diverging land plants. *Development*, *138*(11), 2273–2281. https://doi.org/10.1242/dev.060582

Jung, H., Kim, J. H., Shin, K. D., Kim, J., Lee, H. N., & Chung, T. (2017). Autophagic flux analysis of Arabidopsis seedlings exposed to salt stress. *Journal of Plant Biology*, *60*(2), 199–206. https://doi.org/10.1007/s12374-016-0448-y

Kang, S., Shin, K. D., Kim, J. H., & Chung, T. (2018). Autophagy-related (ATG) 11, ATG9 and the phosphatidylinositol 3-kinase control ATG2-mediated formation of autophagosomes in Arabidopsis. *Plant Cell Reports*, *37*(4), 653–664. https://doi.org/10.1007/s00299-018-2258-9

Kanne, J. V., Ishikawa, M., Bressendorff, S., Ansbøl, J., Hasebe, M., Rodriguez, E., & Petersen, M. (2022). Overexpression of ATG8/LC3 enhances wound-induced somatic reprogramming in Physcomitrium patens. *Autophagy*, *18*(6), 1463–1466. https://doi.org/10.1080/15548627.2021.1975913

Kroemer, G., Mariño, G., & Levine, B. (2010). Autophagy and the Integrated Stress Response. *Molecular Cell*, *40*(2), 280–293. https://doi.org/10.1016/j.molcel.2010.09.023

Kürschner, H. (2004). Life Strategies and Adaptations in Bryophytes from the Near and Middle East. *Turkish Journal of Botany*, *28*(1), 73–84. https://doi.org/-

Landberg, K., Šimura, J., Ljung, K., Sundberg, E., & Thelander, M. (2021). Studies of moss reproductive development indicate that auxin biosynthesis in apical stem cells may constitute an ancestral function for focal growth control. *The New Phytologist*, *229*(2), 845–860. https://doi.org/10.1111/nph.16914

Li, F., Chung, T., Pennington, J. G., Federico, M. L., Kaeppler, H. F., Kaeppler, S. M., Otegui, M. S., & Vierstra, R. D. (2015). Autophagic Recycling Plays a Central Role in Maize Nitrogen Remobilization. *The Plant Cell*, *27*(5), 1389–1408. https://doi.org/10.1105/tpc.15.00158

Li, F., Chung, T., & Vierstra, R. D. (2014). AUTOPHAGY-RELATED11 Plays a Critical Role in General Autophagy- and Senescence-Induced Mitophagy in Arabidopsis. *The Plant Cell*, *26*(2), 788–807. https://doi.org/10.1105/tpc.113.120014

Lin, L.-Y., Chow, H.-X., Chen, C.-H., Mitsuda, N., Chou, W.-C., & Liu, T.-Y. (2023). Role of autophagy-related proteins ATG8f and ATG8h in the maintenance of autophagic activity in Arabidopsis roots under phosphate starvation. *Frontiers in Plant Science*, *14*. https://doi.org/10.3389/fpls.2023.1018984

Liu, Y., Schiff, M., Czymmek, K., Tallóczy, Z., Levine, B., & Dinesh-Kumar, S. P. (2005). Autophagy Regulates Programmed Cell Death during the Plant Innate Immune Response. *Cell*, *121*(4), 567–577. https://doi.org/10.1016/j.cell.2005.03.007

Liu, Y., Xiong, Y., & Bassham, D. C. (2009). Autophagy is required for tolerance of drought and salt stress in plants. *Autophagy*, *5*(7), 954–963. https://doi.org/10.4161/auto.5.7.9290

Ludwig-Müller, J., Jülke, S., Bierfreund, N. M., Decker, E. L., & Reski, R. (2009). Moss (Physcomitrella patens) GH3 proteins act in auxin homeostasis. *New Phytologist*, *181*(2), 323–338. https://doi.org/10.1111/j.1469-8137.2008.02677.x

Lüth, V. M., Rempfer, C., van Gessel, N., Herzog, O., Hanser, M., Braun, M., Decker, E. L., & Reski, R. (2023). A Physcomitrella PIN protein acts in spermatogenesis and sporophyte retention. *New Phytologist*, *237*(6), 2118–2135. https://doi.org/10.1111/nph.18691

Marshall, R. S., & Vierstra, R. D. (2018). Autophagy: The Master of Bulk and Selective Recycling. *Annual Review of Plant Biology*, *69*(Volume 69, 2018), 173–208. https://doi.org/10.1146/annurev-arplant-042817-040606

McDaniel, S. F. (2021). Bryophytes are not early diverging land plants. *New Phytologist*, *230*(4), 1300–1304. https://doi.org/10.1111/nph.17241

Menand, B., Yi, K., Jouannic, S., Hoffmann, L., Ryan, E., Linstead, P., Schaefer, D. G., & Dolan, L. (2007a). An Ancient Mechanism Controls the Development of Cells with a Rooting Function in Land Plants. *Science*, *316*(5830), 1477–1480. https://doi.org/10.1126/science.1142618

Menand, B., Calder, G., & Dolan, L. (2007b). Both chloronemal and caulonemal cells expand by tip growth in the moss Physcomitrella patens. *Journal of Experimental Botany*, *58*(7), 1843–1849. https://doi.org/10.1093/jxb/erm047

Naramoto, S., Hata, Y., Fujita, T., & Kyozuka, J. (2022). The bryophytes Physcomitrium patens and Marchantia polymorpha as model systems for studying evolutionary cell and developmental biology in plants. *The Plant Cell*, *34*(1), 228–246. https://doi.org/10.1093/plcell/koab218

Nemec-Venza, Z., Madden, C., Stewart, A., Liu, W., Novák, O., Pěnčík, A., Cuming, A. C., Kamisugi, Y., & Harrison, C. J. (2022). CLAVATA modulates auxin homeostasis and transport to regulate stem cell identity and plant shape in a moss. *New Phytologist*, *234*(1), 149–163. https://doi.org/10.1111/nph.17969

Petersen, M., Avin-Wittenberg, T., Bassham, D. C., Dagdas, Y., Fan, C., Fernie, A. R., Jiang, L., Mishra, D., Otegui, M. S., Rodriguez, E., & Hofius, D. (2024). Autophagy in plants. *Autophagy Reports*, *3*(1), 2395731. https://doi.org/10.1080/27694127.2024.2395731

Pettinari, G., Finello, J., Plaza Rojas, M., Liberatore, F., Robert, G., Otaiza-González, S., Velez, P., Theumer, M., Agudelo-Romero, P., Enet, A., González, C., Lascano, R., & Saavedra, L. (2022). Autophagy modulates growth and development in the moss Physcomitrium patens. *Frontiers in Plant Science*, *13*. https://doi.org/10.3389/fpls.2022.1052358

Pires, N. D., Yi, K., Breuninger, H., Catarino, B., Menand, B., & Dolan, L. (2013). Recruitment and remodeling of an ancient gene regulatory network during land plant evolution. *Proceedings of the National Academy of Sciences*, *110*(23), 9571–9576. https://doi.org/10.1073/pnas.1305457110

Prigge, M. J., & Bezanilla, M. (2010). Evolutionary crossroads in developmental biology: Physcomitrella patens. *Development*, *137*(21), 3535–3543. https://doi.org/10.1242/dev.049023

Rensing, S. A., Goffinet, B., Meyberg, R., Wu, S.-Z., & Bezanilla, M. (2020). The Moss Physcomitrium (Physcomitrella) patens: A Model Organism for Non-Seed Plants. *The Plant Cell*, *32*(5), 1361–1376. https://doi.org/10.1105/tpc.19.00828

Rodriguez, E., Chevalier, J., Olsen, J., Ansbøl, J., Kapousidou, V., Zuo, Z., Svenning, S., Loefke, C., Koemeda, S., Drozdowskyj, P. S., Jez, J., Durnberger, G., Kuenzl, F., Schutzbier, M., Mechtler, K., Ebstrup, E. N., Lolle, S., Dagdas, Y., & Petersen, M. (2020). Autophagy mediates temporary reprogramming and dedifferentiation in plant somatic cells. *The EMBO Journal*, *39*(4), EMBJ2019103315. https://doi.org/10.15252/embj.2019103315

Rose, T. L., Bonneau, L., Der, C., Marty-Mazars, D., & Marty, F. (2006). Starvation-induced expression of autophagy-related genes in Arabidopsis. *Biology of the Cell*, *98*(1), 53–67. https://doi.org/10.1042/BC20040516

Rounds, C. M., & Bezanilla, M. (2013). Growth Mechanisms in Tip-Growing Plant Cells. *Annual Review of Plant Biology*, *64*(1), 243–265. https://doi.org/10.1146/annurev-arplant-050312-120150

Saavedra, L., Catarino, R., Heinz, T., Heilmann, I., Bezanilla, M., & Malhó, R. (2015). Phosphatase and Tensin Homolog Is a Growth Repressor of Both Rhizoid and

Gametophore Development in the Moss Physcomitrella patens. *Plant Physiology*, *169*(4), 2572–2586. https://doi.org/10.1104/pp.15.01197

Sakil, M. A. (2025). Physcomitrium patens: An emerging model for autophagy study. *Protoplasma*. https://doi.org/10.1007/s00709-025-02148-9

Sanchez-Vera, V., Kenchappa, C. S., Landberg, K., Bressendorff, S., Schwarzbach, S., Martin, T., Mundy, J., Petersen, M., Thelander, M., & Sundberg, E. (2017). Autophagy is required for gamete differentiation in the moss Physcomitrella patens. *Autophagy*, *13*(11), 1939–1951. https://doi.org/10.1080/15548627.2017.1366406

Sheldrake, A. R. (2021). The production of auxin by dying cells. *Journal of Experimental Botany*, *72*(7), 2288–2300. https://doi.org/10.1093/jxb/erab009

Signorelli, S., Tarkowski, Ł. P., Ende, W. V. den, & Bassham, D. C. (2019). Linking Autophagy to Abiotic and Biotic Stress Responses. *Trends in Plant Science*, *24*(5), 413–430. https://doi.org/10.1016/j.tplants.2019.02.001

Slavikova, S., Ufaz, S., Avin-Wittenberg, T., Levanony, H., & Galili, G. (2008). An autophagy-associated Atg8 protein is involved in the responses of Arabidopsis seedlings to hormonal controls and abiotic stresses. *Journal of Experimental Botany*, *59*(14), 4029–4043. https://doi.org/10.1093/jxb/ern244

Suttangkakul, A., Li, F., Chung, T., & Vierstra, R. D. (2011). The ATG1/ATG13 Protein Kinase Complex Is Both a Regulator and a Target of Autophagic Recycling in Arabidopsis. *The Plant Cell*, *23*(10), 3761–3779. https://doi.org/10.1105/tpc.111.090993

Thelander, M., Landberg, K., & Sundberg, E. (2018). Auxin-mediated developmental control in the moss Physcomitrella patens. *Journal of Experimental Botany*, *69*(2), 277–290. https://doi.org/10.1093/jxb/erx255

Thelander, M., Landberg, K., & Sundberg, E. (2019). Minimal auxin sensing levels in vegetative moss stem cells revealed by a ratiometric reporter. *New Phytologist*, *224*(2), 775–788. https://doi.org/10.1111/nph.16068

Thelander, M., Olsson, T., & Ronne, H. (2004). Snf1-related protein kinase 1 is needed for growth in a normal day–night light cycle. *The EMBO Journal*, *23*(8), 1900–1910. https://doi.org/10.1038/sj.emboj.7600182

Thelander, M., Olsson, T., & Ronne, H. (2005). Effect of the energy supply on filamentous growth and development in Physcomitrella patens. *Journal of Experimental Botany*, *56*(412), 653–662. https://doi.org/10.1093/jxb/eri040

Thirumalaikumar, V. P., Wagner, M., Balazadeh, S., & Skirycz, A. (2021). Autophagy is responsible for the accumulation of proteogenic dipeptides in response to heat stress in Arabidopsis thaliana. *The FEBS Journal*, *288*(1), 281–292. https://doi.org/10.1111/febs.15336

Üstün, S., Hafrén, A., & Hofius, D. (2017). Autophagy as a mediator of life and death in plants. *Current Opinion in Plant Biology*, *40*, 122–130. https://doi.org/10.1016/j.pbi.2017.08.011

Viaene, T., Landberg, K., Thelander, M., Medvecka, E., Pederson, E., Feraru, E., Cooper, E. D., Karimi, M., Delwiche, C. F., Ljung, K., Geisler, M., Sundberg, E., & Friml, J. (2014). Directional Auxin Transport Mechanisms in Early Diverging Land Plants. *Current Biology*, *24*(23), 2786–2791. https://doi.org/10.1016/j.cub.2014.09.056

Vidali, L., & Bezanilla, M. (2012). *Physcomitrella patens*: A model for tip cell growth and differentiation. *Current Opinion in Plant Biology*, *15*(6), 625–631. https://doi.org/10.1016/j.pbi.2012.09.008

Wang, Q.-H., Zhang, J., Liu, Y., Jia, Y., Jiao, Y.-N., Xu, B., & Chen, Z.-D. (2022). Diversity, phylogeny, and adaptation of bryophytes: Insights from genomic and transcriptomic data. *Journal of Experimental Botany*, *73*(13), 4306–4322. https://doi.org/10.1093/jxb/erac127

Wang, S., & Blumwald, E. (2014). Stress-Induced Chloroplast Degradation in Arabidopsis Is Regulated via a Process Independent of Autophagy and Senescence-Associated Vacuoles. *The Plant Cell*, *26*(12), 4875–4888. https://doi.org/10.1105/tpc.114.133116

Wang, Y., Yu, B., Zhao, J., Guo, J., Li, Y., Han, S., Huang, L., Du, Y., Hong, Y., Tang, D., & Liu, Y. (2013). Autophagy Contributes to Leaf Starch Degradation. *The Plant Cell*, *25*(4), 1383–1399. https://doi.org/10.1105/tpc.112.108993

Yan, H., Zhuang, M., Xu, X., Li, S., Yang, M., Li, N., Du, X., Hu, K., Peng, X., Huang, W., Wu, H., Tse, Y. C., Zhao, L., & Wang, H. (2023). Autophagy and its mediated mitochondrial quality control maintain pollen tube growth and male fertility in Arabidopsis. *Autophagy*, *19*(3), 768–783. https://doi.org/10.1080/15548627.2022.2095838

Zhuang, X., & Jiang, L. (2019). Chloroplast Degradation: Multiple Routes Into the Vacuole. *Frontiers in Plant Science*, *10*. https://doi.org/10.3389/fpls.2019.00359

FIGURES

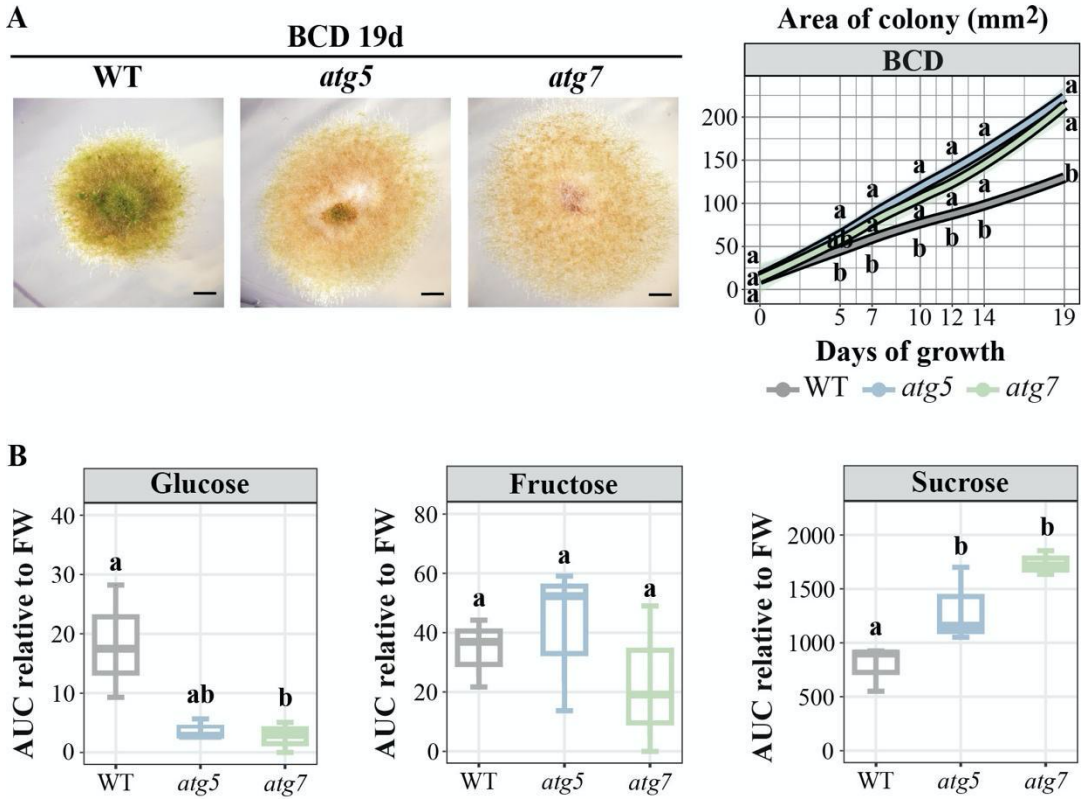

Figure 1. In the absence of ammonium, *atg* mutants show further colony expansion and changes in sugar content. A) Colony spread analysis of WT, *atg5* and *atg7* genotypes growing in BCD medium (-NH_4^+, +NO_3^-). Images were taken at the end of the experiment (19 days). Scale bar: 2 mm. Different letters indicate significant differences between genotypes at each time point (*n*= 9, One-way ANOVA and Tukey's HSD test; P < 0.05) B) Quantification of soluble sugars via HPLC in 7-day-old protonemata of WT, *atg5* and *atg7* lines grown in BCD. AUC: area under the curve. Different letters indicate significant differences between genotypes (*n*= 3, One-way ANOVA and Tukey's HSD test; P < 0.05).

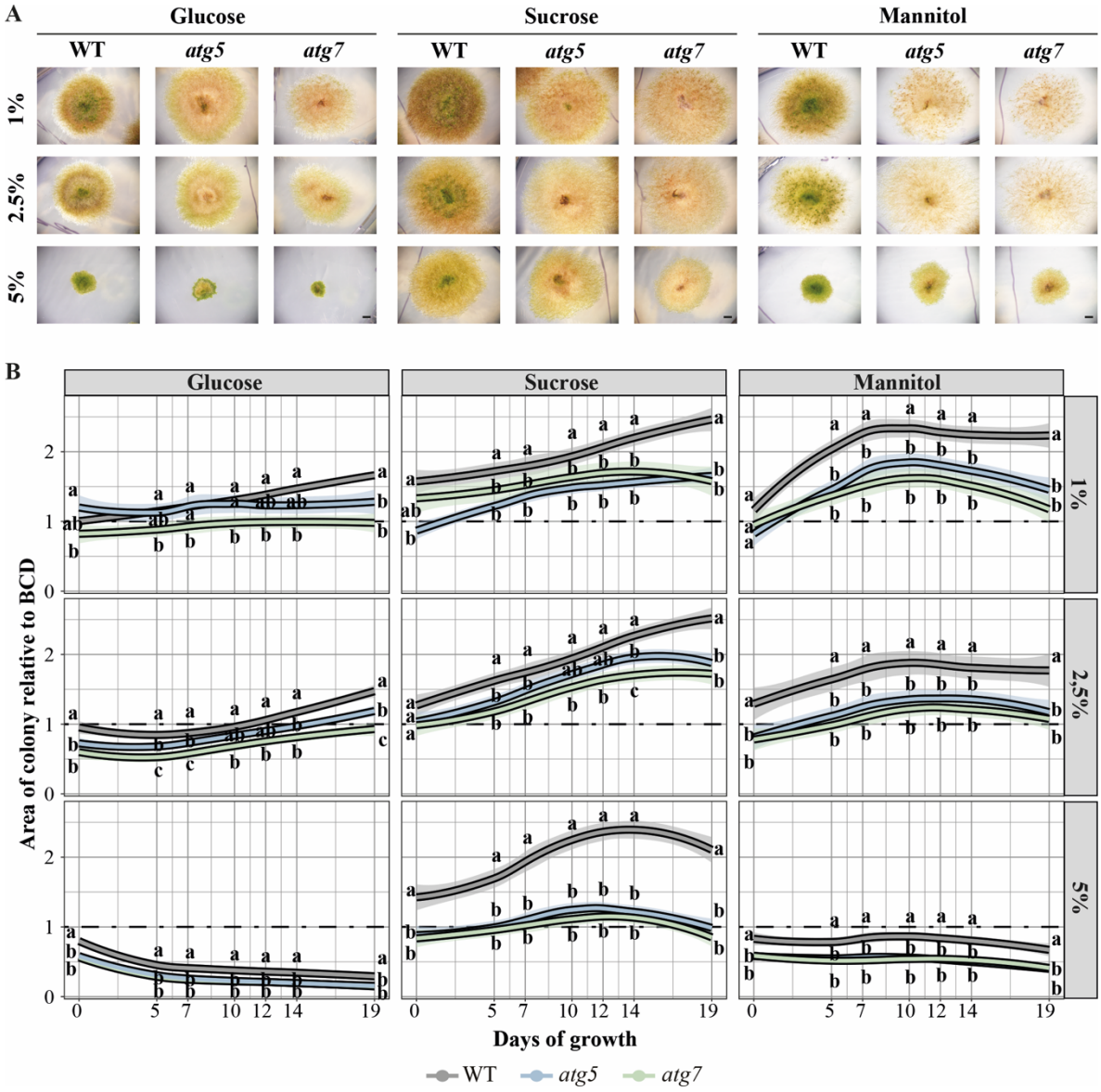

Figure 2. Sugar sensitivity is altered in mutants with impaired autophagy. A) Representative images of WT, *atg5* and *atg7* colonies after 19d of growth in BCD medium supplemented with 1%, 2.5% and 5% glucose, sucrose or mannitol. Scale bar: 2 mm. B) Colony spread analysis of colonies shown in A. For each timepoint, area is shown as relative to BCD without supplementation (for each genotype). Different letters indicate significant differences between genotypes at each time point (*n*= 9, One-way ANOVA and Tukey's HSD test; $P < 0.05$)

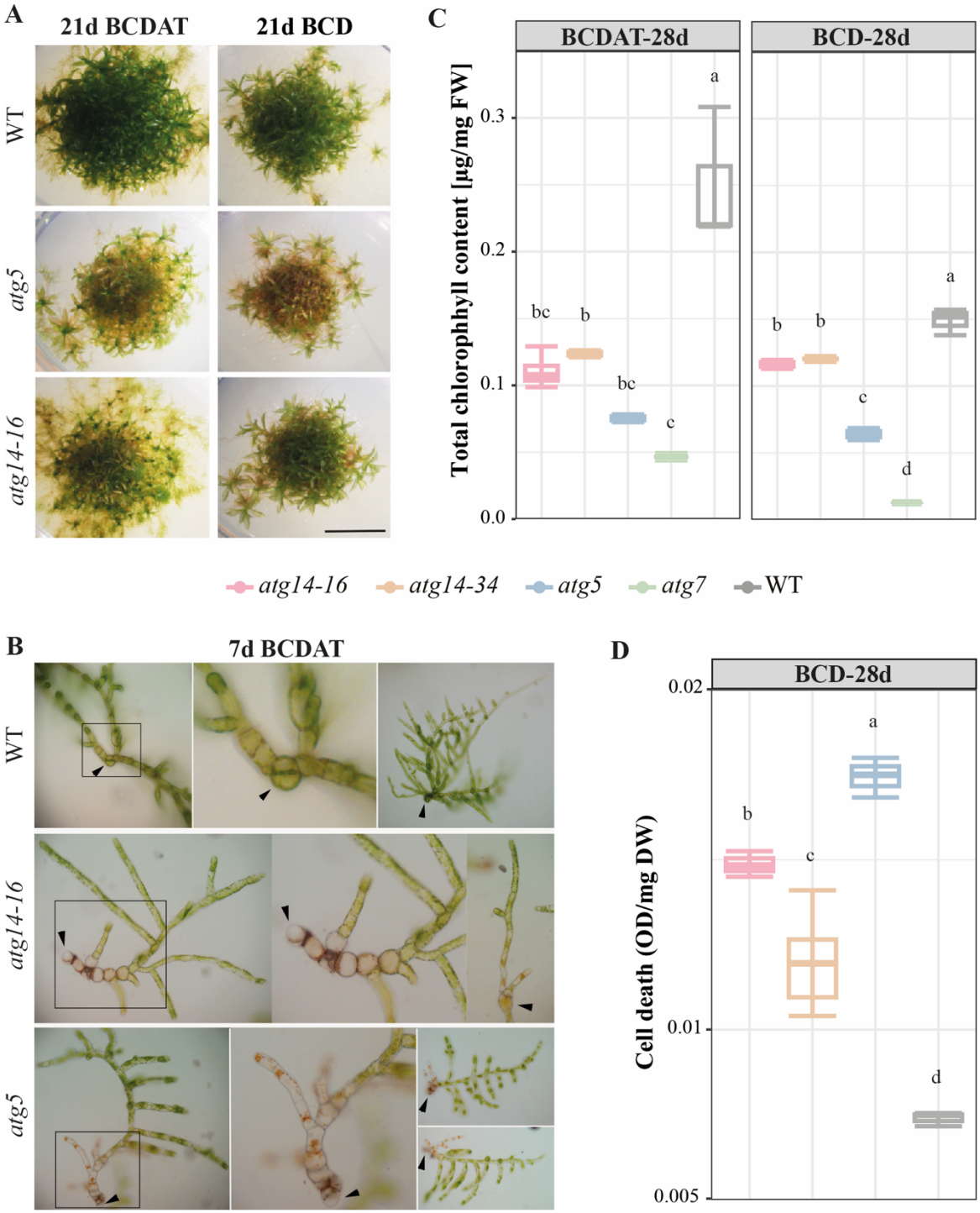

Figure 3. Mutants lacking PpATG14 show an intermediate phenotype between the WT and *atg5* mutants. A) Representative images of WT, atg5 and atg14 colonies after 21 days of growth in BCDAT ($+NH_4^+$, $+NO_3^-$) and BCD ($-NH_4^+$, $+NO_3^-$). Scale bar: 6 mm. B) Representative images of filaments regenerated from protopasts after 7 days of growth in BCDAT medium. Squares highlight senescent areas in the center part of the regenerating filaments from *atg5* and *atg14* genotypes, in contrast to the WT. Black arrowheads indicate the oldest cell in the filament. C) Total chlorophyll content in WT, atg5, atg7 and two independent *atg14* (*atg14-16* and *atg14-34*) lines. Quantification was carried out in colonies after 28 days of growth in

BCDAT and BCD media. Different letters indicate significant differences between genotypes (*n*= 3, One-way ANOVA and Tukey's HSD test; P < 0.05). D) Cell death quantification using Evans Blue in WT, *atg5* and *atg14* colonies after 28 days of growth in BCD. Different letters indicate significant differences between genotypes (*n*= 3, One-way ANOVA and Tukey's HSD test; P < 0.05).

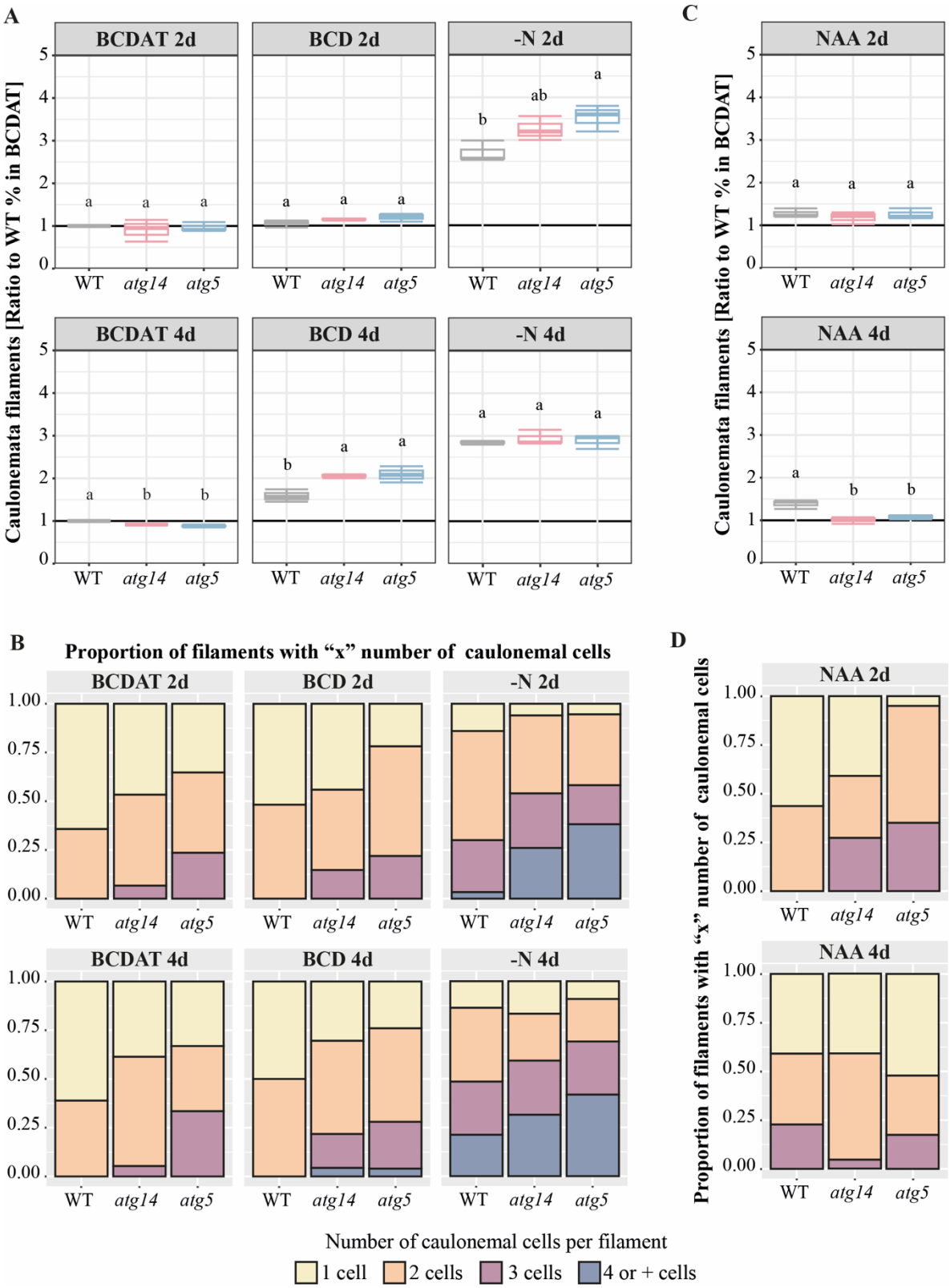

Figure 4. Caulonemata development in *atg* mutants responds differently to nitrogen deficiency and auxin treatment. A) Protoplasts regeneration assay showing the percentage of caulonemata filaments in WT, *atg14* and *atg5* genotypes after 2 or 4 days of transference to BCDAT ($+NH_4^+$, $+NO_3^-$ -nutrient rich-, control), BCD ($-NH_4^+$, $+NO_3^-$) and -N ($-NH_4^+$, $-NO_3$). For each timepoint, values for every treatment and genotype are shown as relative to the percentage of the WT in BCDAT (control situation). For each treatment and timepoint, different letters indicate significant differences between genotypes (*n*= 40, One-way ANOVA and Tukey's HSD test; $P < 0.05$). B) Proportion of caulonemata filaments with a given number of caulonemal cells after transference to BCDAT, BCD or -N. Caulonemata filaments identified in A were categorized according to the number of caulonemata cells present in each filament. C) Protoplasts regeneration assay showing the percentage of caulonemata filaments in WT, *atg14* and *atg5* genotypes after 2 or 4 days of transference to BCDAT supplemented with NAA 1µM. For each timepoint, values for every treatment and genotype are shown as relative to the percentage of the WT in BCDAT (control situation), and different letters indicate significant differences between genotypes (*n*= 40, One-way ANOVA and Tukey's HSD test; $P < 0.05$). D) Proportion of caulonemata filaments with a given number of caulonemal cells after transference to BCDAT supplemented with NAA 1µM.

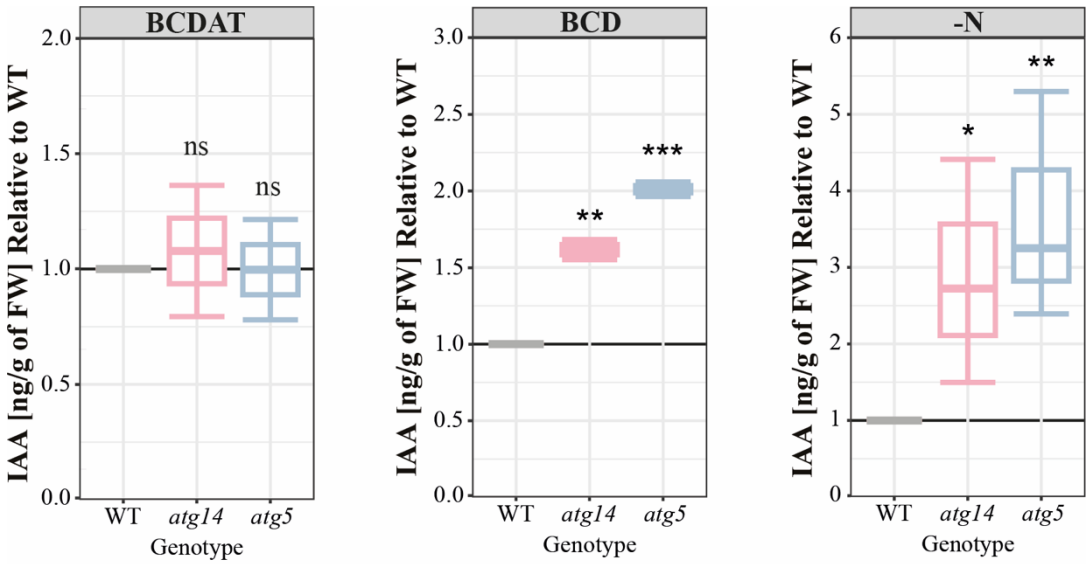

Figure 5. IAA accumulates in *atg* mutants after transference to mild and complete nitrogen deficiencies. IAA content in protonemata was measured after 3 days of transference to BCDAT ($+NH_4^+$, $+NO_3^-$ -nutrient rich-, control), BCD ($-NH_4^+$, $+NO_3^-$) and -N ($-NH_4^+$, $-NO_3$). For each condition, asterisks indicate significant differences between each *atg* mutant and the WT (*n*= 3, T test; *= $P < 0.1$, **= $P < 0.05$, ***= $P < 0.01$). In each treatment, values for every genotype are shown as relative to the WT within the same treatment.

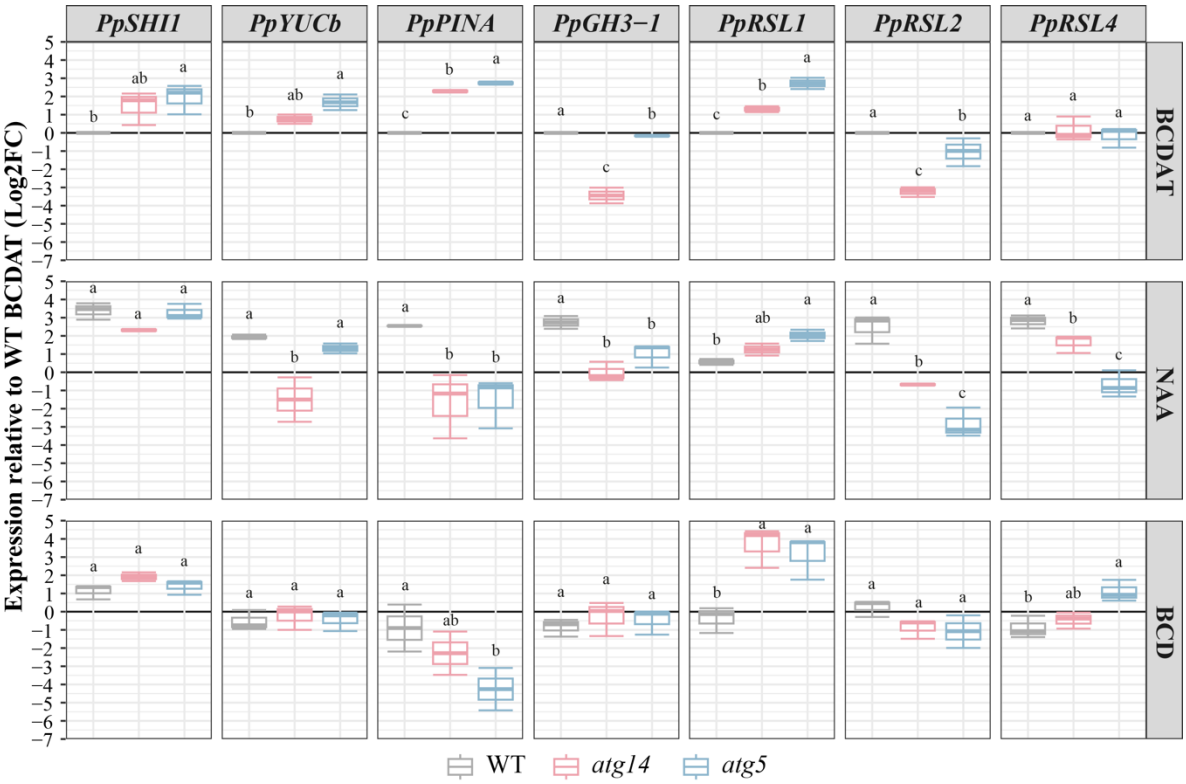

Figure 6. Expression of auxin-related genes is altered in mutants with impaired autophagy. Quantification of gene expression by RT-qPCR in WT, *atg5* and *atg14* protonemata after transference to BCDAT ($+NH_4^+$, $+NO_3^-$ -nutrient rich-, control), and BCD ($-NH_4^+$, $+NO_3^-$) or NAA 5µM treatment. For each gene and condition, values are shown as relative to the WT in BCDAT, and different letters indicate significant differences between genotypes (*n*= 3, One-way ANOVA and Tukey's HSD test; $P < 0.05$).

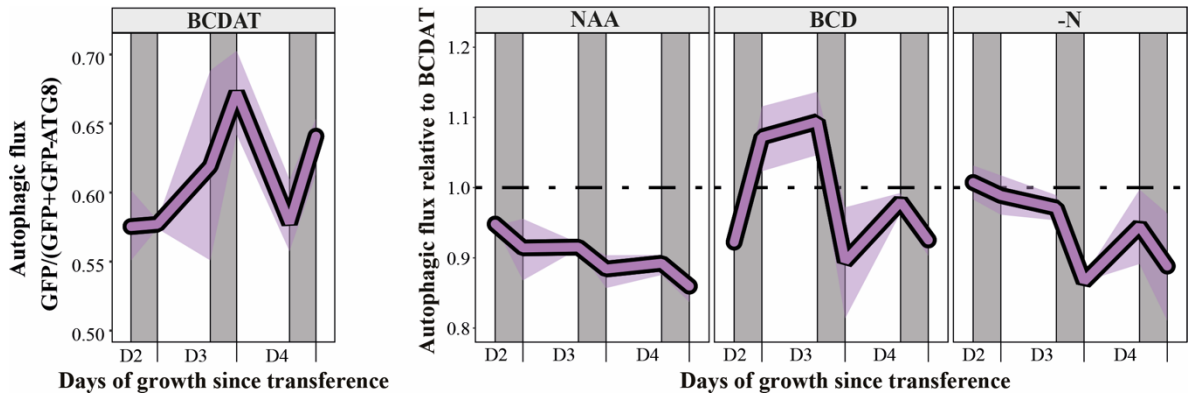

Figure 7. Autophagic flux decreases after transference to caulonemata-inducing conditions. GFP-ATG8e cleavage assay by Western blot in protonemata transferred to different caulonemata-inducing conditions. Light and dark hours of a 16:8 photoperiod are represented by the white and grey areas, respectively. Left panel: BCDAT ($+NH_4^+$, $+NO_3^-$ -nutrient rich-, control). Right panel: NAA 1µM, BCD ($-NH_4^+$, $+NO_3^-$) and -N ($-NH_4^+$, $-NO_3$), values are shown as relative to BCDAT.

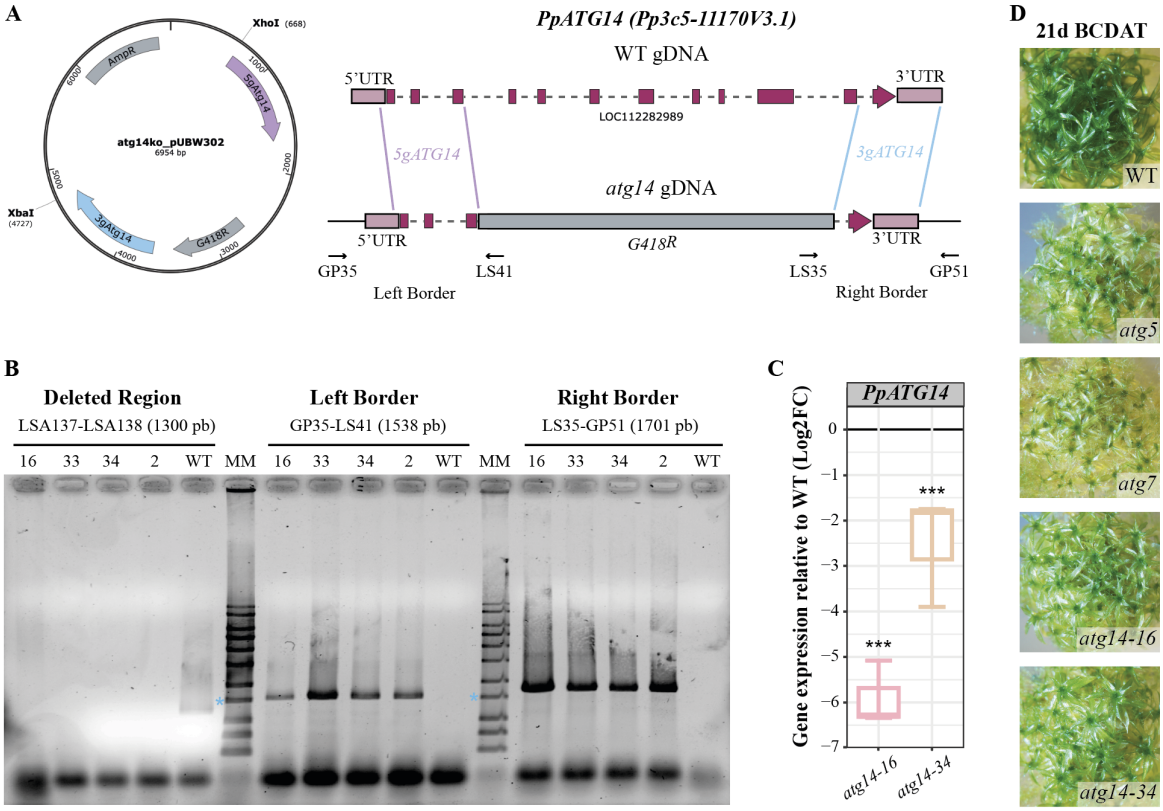

Figure S1. Generation and genotyping of *Ppatg14* mutant lines. A) Vector used for protoplast transformation, indicating the restriction enzymes used for linearization (left). Schematic representation of genomic DNA from WT plants and *atg14* mutants, showing the exon structure of PpATG14 and the replaced region (right). B) Genotyping of four independent *atg14* lines. Light blue asterisks indicate the 1500 bp marker band. C) Relative *PpATG14* transcript levels in *atg14-16* and *atg14-34* lines determined by RT–qPCR. Values are expressed relative to WT (black line) and represent mean ± s.d. of biological replicates (n = 3). ***p < 0.01 (Student's *t*-test vs WT). D) Colony phenotype of WT, *atg5*, *atg7*, and two independent *atg14* lines (*atg14-16* and *atg14-34*) after 21 days of growth on BCDAT medium.

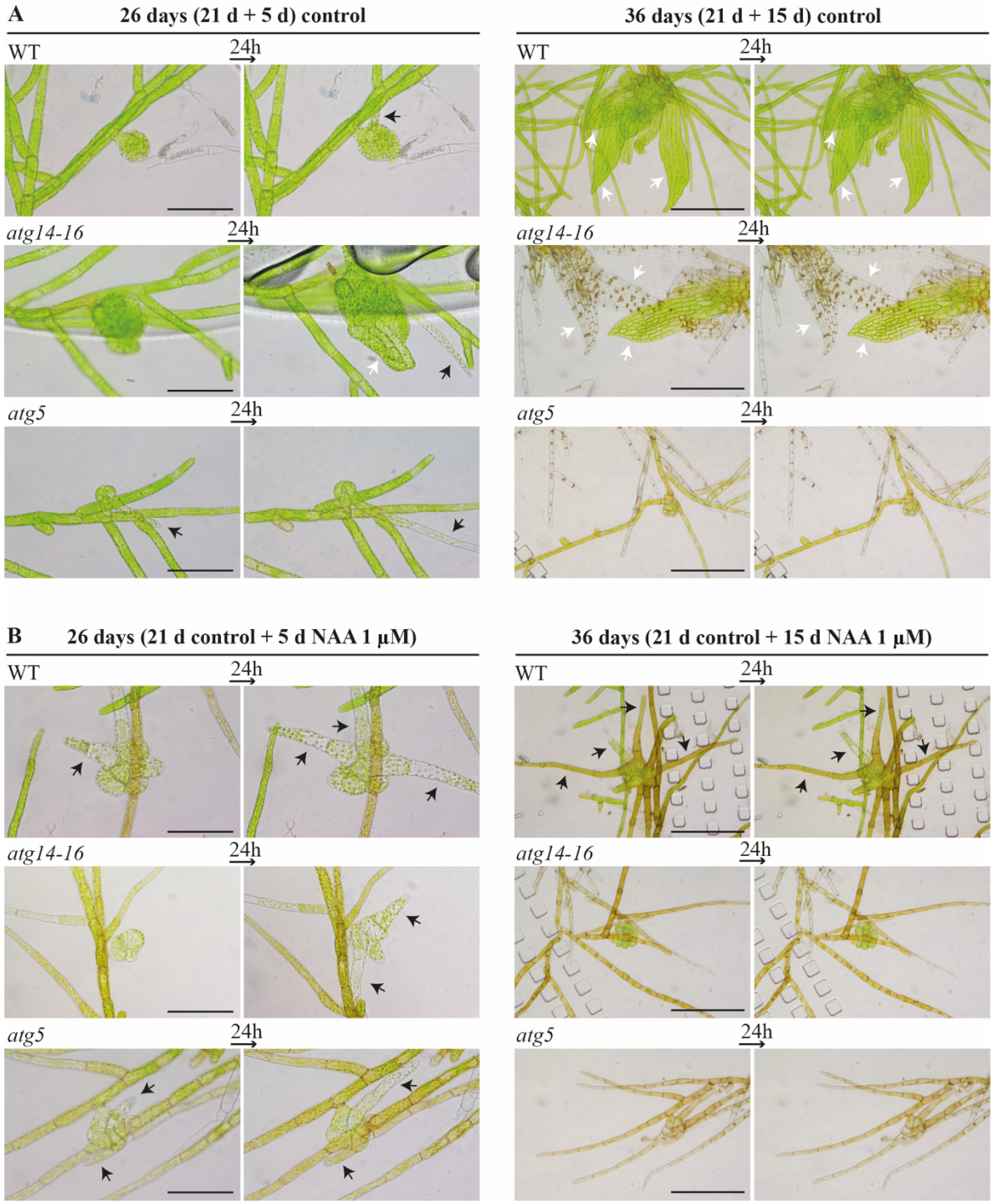

Figure S2. *atg* mutants display hypersensitivity to auxins. Tissue from WT, *atg14-16*, and *atg5* lines grown in microfluidic chambers for 21 days under control conditions and for an additional 5 (left panels) or 15 (right panels) days on BCDAT media (A) or supplemented with 1 µM NAA (B). Scale bars: 200 µm (left panels) and 500 µm (right panels). Black arrows indicate rhizoids, and white arrows indicate phyllids.